

Reconstruction of global surface ocean $p\text{CO}_2$ using region-specific predictors based on a stepwise FFNN regression algorithm

Guorong Zhong^{1,2,3,4}, Xuegang Li^{1,2,3,4*}, Jinming Song^{1,2,3,4*}, Baoxiao Qu^{1,3,4}, Fan Wang^{1,2,3,4}, Yanjun Wang^{1,4}, Bin Zhang^{1,4}, Xiaoxia Sun^{1,2,3,4}, Wuchang Zhang^{1,3,4}, Zhenyan Wang^{1,3,4}, Jun Ma^{1,3,4}, Huamao Yuan^{1,2,3,4}, Liqin Duan^{1,2,3,4}

¹Institute of Oceanology, Chinese Academy of Sciences, Qingdao 266071, China

²University of Chinese Academy of Sciences, Beijing 101407, China

³Pilot National Laboratory for Marine Science and Technology, Qingdao 266237, China

⁴Center for Ocean Mega-Science, Chinese Academy of Sciences, Qingdao 266071, China

Correspondence to: Xuegang Li (lixuegang@qdio.ac.cn); Jinming Song (jmsong@qdio.ac.cn)

Abstract: Various machine learning methods were attempted in the global mapping of surface ocean partial pressure of CO_2 ($p\text{CO}_2$) to reduce the uncertainty of global ocean CO_2 sink estimate due to undersampling of $p\text{CO}_2$. In previous researches, the predictors of $p\text{CO}_2$ were usually selected empirically based on theoretic drivers of surface ocean $p\text{CO}_2$, and the same combination of predictors were was applied in all areas unless lack of coverage. However, the differences between the drivers of surface ocean $p\text{CO}_2$ in different regions were not considered. In this work, we combined the stepwise regression algorithm and a Feed-Forward Neural Network (FFNN) to selected predictors of $p\text{CO}_2$ based on the mean absolute error in each of the 11 biogeochemical provinces defined by the Self-Organizing Map (SOM) method. Based on the predictors selected, a monthly global $1^\circ \times 1^\circ$ surface ocean $p\text{CO}_2$ product from January 1992 to August 2019 was constructed. Validation of different combinations of predictors based on the SOCAT dataset version 2020 and independent observations from time-series stations was carried out. The prediction of $p\text{CO}_2$ based on region-specific predictors selected by the stepwise FFNN algorithm were was more precise than that based on predictors from previous researches. Applying of a the FFNN size improving algorithm in each province decreased the mean absolute error (MAE) of the global estimate to $11.32 \mu\text{atm}$ and the root mean square error (RMSE) to $17.99 \mu\text{atm}$. The script file of the stepwise FFNN algorithm and $p\text{CO}_2$ product are distributed through the Institute of Oceanology of the Chinese Academy of Sciences Marine Science Data Center (IOCAS; <http://dx.doi.org/10.12157/iocas.2021.0022>, Zhong et al., 2021).

1 Introduction

As a net sink for atmospheric CO₂, global oceans ~~have been thought to~~ have removed about ~~one one~~-third of anthropogenic CO₂ since the beginning of the industrial revolution (Sabine et al., 2004; Friedlingstein et al., 2019). However, ~~, due to large uncertainty in estimates of surface ocean partial pressure of CO₂ (pCO₂), the long-term average~~ global ocean sea-air CO₂ flux ~~averaged between during 2001-2015 estimated based on sea-air pCO₂ difference varies~~ differ from -1.55 to -1.74 PgC yr⁻¹ ~~with the maximum difference in individual years nearly 0.6 PgC yr⁻¹, depending on the surface ocean partial pressure of CO₂ (pCO₂) product and the maximum difference between global sea-air CO₂ flux in individual years reached nearly 0.6 PgC yr⁻¹. These differences largely stem from differences in pCO₂ estimates across the products~~ (Rödenbeck et al., 2014; Iida et al., 2015; Landschützer et al., 2014; Denvil-Sommer et al., 2019). The magnitude and direction of the flux ~~is are~~ primarily ~~largely~~ set by the air-sea pCO₂ difference. ~~Surface water pCO₂ greater than the overlying air indicates CO₂ is released from the ocean to the air. Conversely, absorption of CO₂ by oceans happens when the pCO₂ of the surface water is lower than the overlying air. Greater pCO₂ of surface water than that of overlying air indicating that CO₂ released from oceans to the air, and absorption of CO₂ by oceans happened when the pCO₂ of surface water was lower than that of air.~~ The ocean in these two scenarios is known as oceanic carbon source and oceanic carbon sink, respectively.

Sparse and uneven observations of surface ocean pCO₂ in time and space severely limited the understanding of interannual variability of oceanic carbon sink, and researches based on different methods were carried out to break this barrier. In earlier studies, traditional unitary and multiple regression methods between surface ocean pCO₂ and its drivers ~~was were~~ attempted in the mapping of surface ocean pCO₂, which were limited in specific regions and sometimes even in ~~particular specific~~ seasons with a relatively high root mean square error (RMSE) (Sarma et al., 2006; Takahashi et al., 2006; Shadwick et al., 2010; Chen et al., 2011; Marrec et al., 2015). ~~Advances in Recent researches on~~ artificial neural networks and other machine learning algorithms, such as ~~the~~ feed-forward neural network (FFNN) method (Zeng et al., 2014; Zeng et al., 2015; Moussa et al., 2016; Denvil-Sommer et al., 2019) and self-organization mapping (SOM) method (Friedrich and Oschlies, 2009; Telszewski et al., 2009; Hales et al., 2012; Nakaoka et al., 2013), significantly reduced the bias in the interpolation based on relationships between surface ocean pCO₂ and its drivers. In addition, ~~methods such as~~ finding better predictors or combining SOM ~~and with~~ other neural networks ~~were was~~

also attempted ~~to further~~ decrease the $p\text{CO}_2$ predicting error ~~further~~ (Hales et al., 2012; Nakaoka et al., 2013; Landschützer et al., 2014; Chen et al., 2019; Denvil-Sommer et al., 2019; Zhong et al., 2020; Wang et al., 2021). However, the selection of predictors in the surface ocean $p\text{CO}_2$ mapping was more empirical, focusing on the theoretical drivers of the $p\text{CO}_2$ and its variation. Sea surface temperature and salinity, related to the solubility of CO_2 in seawater, ~~were~~ are considered as the most important and used in almost all related studies (Landschützer et al., 2013; Nakaoka et al., 2013; Moussa et al., 2016; Laruelle et al., 2017; Zeng et al., 2017; Denvil-Sommer et al., 2019). Similarly, the chlorophyll-a concentration is also widely used (Nakaoka et al., 2013; Landschützer et al., 2014; Laruelle et al., 2017; Zeng et al., 2017; Denvil-Sommer et al., 2019), which is related to the phytoplankton uptake of CO_2 . One more ~~indicator~~ predictor, mixed layer depth, ~~frequently appeared~~ appears frequently in ~~related~~ associated studies as a proxy related to the vertical transport of dissolved carbon (Telszewski et al., 2009; Nakaoka et al., 2013; Landschützer et al., 2014; Zeng et al., 2017; Denvil-Sommer et al., 2019). ~~In addition, sampling information, such as latitude and longitude~~ Besides, the sampling information have been also used as indicators, including latitude and longitude (Friedrich and Oschlies, 2009; Jo et al., 2012; Zeng et al., 2015; Zeng et al., 2017; Denvil-Sommer et al., 2019; Gregor et al. 2019), and sampling time (Friedrich and Oschlies, 2009; Zeng et al., 2015), has been used as a predictor. In recent researches, ~~the~~ dry air mixing ratio of atmospheric CO_2 ($x\text{CO}_2$), related to the CO_2 level in ~~the~~ air, was also used ~~as a predictor of to predict~~ surface ocean $p\text{CO}_2$ (Landschützer et al., 2014; Denvil-Sommer et al., 2019). The sea surface height, which was considered effective in improving the spatial pattern and the accuracy of surface ocean $p\text{CO}_2$ mapping at the basin and regional scale, and the monthly anomalies of the most widely used predictors ~~parameters~~ mentioned above were used by the Denvil-Sommer et al. (2019). In the research focus inged on the surface ocean $p\text{CO}_2$ mapping of coastal areas, the bathymetry, sea ice, and wind speed were also used as predictors ~~indicators~~ (Laruelle et al., 2017). In each of these researches, ~~the~~ same combination of predictors ~~indicators~~ was applied in all ~~areas of the~~ global ocean areas, although the global ocean was divided into several biogeochemical provinces in some of the researches. However, the predictor indicator that plays an vital important role in the surface ocean $p\text{CO}_2$ reconstruction at one region may ~~be not~~ be a good predictor of surface ocean $p\text{CO}_2$ in ~~the~~ other regions, due to complex and variable drivers ~~in different regions~~. Nevertheless, ~~But~~ no widely recognized methods for judging the importance of each predictor in the surface ocean $p\text{CO}_2$ mapping are available yet. Thus, we attempted to construct a

stepwise FFNN algorithm to rank the importance of predictors and figure out the optimal combination in each biogeochemical province defined by SOM₇ for decreasing the prediction errors in the surface ocean $p\text{CO}_2$ mapping.

2 Methodology

2.1 Data

The surface ocean fugacity of CO_2 ($f\text{CO}_2$) observation data from the Surface Ocean CO_2 Atlas $f\text{CO}_2$ dataset version 2020 (SOCATv2020) (Bakker et al., 2016) was used to construct the non-linear relationship between surface ocean $p\text{CO}_2$ and predictors. The conversion between $f\text{CO}_2$ and $p\text{CO}_2$ was following the formula (Körtzinger, 1999):

$$f\text{CO}_2 = p\text{CO}_2 \cdot \exp\left(P \cdot \frac{B+2\delta}{RT}\right) \quad (1)$$

where $f\text{CO}_2$ and $p\text{CO}_2$ are in micro-atmospheres (μatm), P is the total atmospheric surface pressure (Pa) using the National Centers for Environmental Prediction (NCEP) monthly mean sea level pressure product (Dee et al., 2011), and T is the absolute temperature (K). R is the gas constant ($8.314 \text{ J K}^{-1} \text{ mol}^{-1}$). Parameters B ($\text{m}^3 \text{ mol}^{-1}$) and δ ($\text{m}^3 \text{ mol}^{-1}$) are both viral coefficients (Weiss, 1974).

In this work, ~~total 33 indicatorpredictors~~ were used (Table S1). ~~W, where 21 were chosen from previous researches of surface ocean $p\text{CO}_2$ reconstruction based on machine learning methods, including sea surface temperature (SST) and sea surface salinity (SSS) using the $1^\circ \times 1^\circ$ gridded product (Cheng et al., 2016; Cheng et al., 2017; Cheng et al., 2020) at <http://www.ocean.iap.ac.cn/> and the anomalies (SST_{anom} and SSS_{anom}), chlorophyll-a concentration (CHL-a) and the anomaly ($\text{CHL-a}_{\text{anom}}$) using satellite derived monthly product in 9 km resolution (NASA Goddard Space Flight Center, Ocean Ecology Laboratory, Ocean Biology Processing Group, 2018), mixed layer depth (MLD) and sea surface height (SSH) and the anomalies (MLD_{anom} and SSH_{anom}) using the ECCO2-cube92 daily product (Menemenlis et al., 2008), dry air mixing ratio of atmospheric CO_2 ($x\text{CO}_2$) and the anomaly ($x\text{CO}_2_{\text{anom}}$) from the GLOBALVIEW marine boundary layer product (GLOBALVIEW CO_2 , 2011), sea ice area fraction using the monthly product from ECMWF ERA Interim (Dee et al., 2011), 10-meters wind speed using the monthly product from ECMWF ERA Interim (Dee et al., 2011), bathymetry from ETOPO2 (Commerce et al., 2006), year and month (represented by 1-12), the total number of months since January 1992 (N_{mon}), the sine of latitude and the sine and cosine of longitude (sLat, sLon and cLon). In addition, 12 parameters-predictors which were only used in similar previous research focused on other-parametersthe mapping of total alkalinity or dissolved inorganic carbon~~

(Broullón et al., 2019; Broullón et al., 2020), or were possibly related to the driver of surface ocean $p\text{CO}_2$ and its variability, were selected to be tested (Predictors with the * label in Table 1). ~~These parameters included nitrate, phosphate, silicate and dissolved oxygen (DO) using the monthly climatology product from WOA18 (Garcia et al., 2019a, b), sea level pressure (SLP) and surface pressure from the ECMWF ERA Interim (Dee et al., 2011), W velocity of ocean currents (W_{vel}) at 5, 65, 105 and 195 m depth using the ECCO2 cube92 3-day product (Menemenlis et al., 2008), the Oceanic Nino Index (ONI) (Huang et al., 2017), the Southern Hemisphere Annular Mode Index (SAM) (Marshall, G. J., 2003).~~ Most of these products were retrieved at $1^\circ \times 1^\circ$ resolution. Some products retrieved at higher resolution were downscaled to $1^\circ \times 1^\circ$ resolution by taking the average of all values in each $1^\circ \times 1^\circ$ grid.

Table 1. Predictors and corresponding data products

<u>Predictor</u>	<u>Abbreviation</u>	<u>Data product</u>	<u>Resolution</u>
<u>Sine of latitude</u>	<u>sLat</u>	=	=
<u>Sine of longitude</u>	<u>sLon</u>	=	=
<u>Cosine of longitude</u>	<u>cLon</u>	=	=
<u>Number of months since January 1992</u>	<u>N_{mon}</u>	=	=
<u>Year</u>	<u>Year</u>	=	=
<u>Month</u>	<u>Month</u>	=	=
<u>Sea surface temperature</u>	<u>SST</u>	<u>Chen et al., 2016; Chen et al., 2017</u>	<u>$1^\circ \times 1^\circ$, monthly, 1940-2021</u>
<u>Monthly anomaly of SST</u>	<u>SST_{anom}</u>	<u>Chen et al., 2016; Chen et al., 2017</u>	<u>$1^\circ \times 1^\circ$, monthly, 1940-2021</u>
<u>Sea surface salinity</u>	<u>SSS</u>	<u>Chen et al., 2020</u>	<u>$1^\circ \times 1^\circ$, monthly, 1940-2021</u>
<u>Monthly anomaly of SSS</u>	<u>SSS_{anom}</u>	<u>Chen et al., 2020</u>	<u>$1^\circ \times 1^\circ$, monthly, 1940-2021</u>
<u>Mixed layer depth</u>	<u>MLD</u>	<u>Menemenlis et al., 2008</u>	<u>$0.25^\circ \times 0.25^\circ$, monthly, 1992-2019</u>
<u>Monthly anomaly of MLD</u>	<u>MLD_{anom}</u>	<u>Menemenlis et al., 2008</u>	<u>$0.25^\circ \times 0.25^\circ$, monthly, 1992-2019</u>
<u>Sea surface height</u>	<u>SSH</u>	<u>Menemenlis et al., 2008</u>	<u>$0.25^\circ \times 0.25^\circ$, monthly, 1992-2019</u>
<u>Monthly anomaly of SSH</u>	<u>SSH_{anom}</u>	<u>Menemenlis et al., 2008</u>	<u>$0.25^\circ \times 0.25^\circ$, monthly, 1992-2019</u>
<u>Sea ice fraction</u>	<u>f_{ice}</u>	<u>Dee et al., 2011</u>	<u>$1^\circ \times 1^\circ$, monthly, 1979-2019</u>
<u>10 m Wind speed</u>	<u>Wind</u>	<u>Dee et al., 2011</u>	<u>$1^\circ \times 1^\circ$, monthly, 1979-2019</u>
<u>dDry air mixing ratio of atmospheric CO₂</u>	<u>xCO₂</u>	<u>GLOBALVIEW-CO₂, 2011</u>	<u>0.25° latitude, monthly, 1979-2019</u>
<u>Monthly anomaly of</u>	<u>xCO₂_{anom}</u>	<u>GLOBALVIEW-CO₂,</u>	<u>0.25° latitude, monthly,</u>

<u>xCO₂</u>		<u>2011</u>	<u>1979-2019</u>
<u>Bathymetry</u>	<u>Bathymetry</u>	<u>Commerce et al., 2006</u>	<u>2'× 2'</u>
<u>Chlorophyll concentration</u>	<u>Chl-a</u>	<u>NASA Ocean Biology Processing Group, 2018</u>	<u>9km×9km, monthly, 2002-2021</u>
<u>Monthly anomaly of CHL</u>	<u>Chl-a_{anom}</u>	<u>NASA Ocean Biology Processing Group, 2018</u>	<u>9km×9km, monthly, 2002-2021</u>
<u>W velocity of ocean currents at 5 m depth*</u>	<u>W_{vel}(5m)</u>	<u>Menemenlis et al., 2008</u>	<u>0.25°× 0.25°, monthly, 1992-2019</u>
<u>W_{vel} at 65 m depth*</u>	<u>W_{vel}(65m)</u>	<u>Menemenlis et al., 2008</u>	<u>0.25°× 0.25°, monthly, 1992-2019</u>
<u>W_{vel} at 105 m depth*</u>	<u>W_{vel}(105m)</u>	<u>Menemenlis et al., 2008</u>	<u>0.25°× 0.25°, monthly, 1992-2019</u>
<u>W_{vel} at 195 m depth*</u>	<u>W_{vel}(195m)</u>	<u>Menemenlis et al., 2008</u>	<u>0.25°× 0.25°, monthly, 1992-2019</u>
<u>Sea level pressure*</u>	<u>SLP</u>	<u>Dee et al., 2011</u>	<u>1°× 1°, monthly, 1979-2019</u>
<u>Surface pressure*</u>	<u>Surface pressure</u>	<u>Dee et al., 2011</u>	<u>1°× 1°, monthly, 1979-2019</u>
<u>Climatology of dissolved oxygen*</u>	<u>DO</u>	<u>Garcia et al., 2019b</u>	<u>1°× 1° in the horizontal, 102 depth levels (0–5500 m) in the vertical and monthly</u>
<u>Climatology of nitrate*</u>	<u>Nitrate</u>	<u>Garcia et al., 2019a</u>	<u>1°× 1° in the horizontal, 102 depth levels (0–5500 m) in the vertical and monthly</u>
<u>Climatology of phosphate*</u>	<u>Phosphate</u>	<u>Garcia et al., 2019a</u>	<u>1°× 1° in the horizontal, 102 depth levels (0–5500 m) in the vertical and monthly</u>
<u>Climatology of silicate*</u>	<u>Silicate</u>	<u>Garcia et al., 2019a</u>	<u>1°× 1° in the horizontal, 102 depth levels (0–5500 m) in the vertical and monthly</u>
<u>Oceanic Nino Index*</u>	<u>ONI</u>	<u>Huang et al., 2017</u>	<u>Monthly, 1950-2021</u>
<u>Southern Hemisphere Annular Mode Index*</u>	<u>SAM</u>	<u>Marshall, G. J., 2003</u>	<u>Monthly, 1957-2021</u>

(Predictors with the * label were first included in the *p*CO₂ mapping, where the climatology of nitrate, phosphate, silicate, and dissolved oxygen were used in the mapping of total alkalinity and dissolved inorganic carbon in previous research. All data products retrieved at the resolution higher than 1°× 1° were downscaled to 1°× 1° resolution.)

2.2 Biogeochemical provinces defined by the Self-Organizing Map

For applying a different combination of ~~indicators~~-predictors in regions based on the differences in the dominated drivers of *p*CO₂ and its variability, the global ocean was divided into a set of biogeochemical provinces using a Self-Organizing Map (SOM)

method. The monthly climatology of temperature, salinity, mixed layer depth, sea surface height, nitrate, phosphate, silicate, and dissolved oxygen and $p\text{CO}_2$ climatology from Landschützer et al., (2020) were put into a 3-by-4 size SOM networks to generate 12 biogeochemical provinces, where the monthly climatology data in all 12 months were put into one SOM network to generate one discrete set of biogeochemical provinces. Provinces with ~~connected pixels~~ less than 10 pixels and ~~provinces with SOCAT observation~~ less than 1000 SOCAT observations were defined as discrete small “island” provinces, and then merged with nearest provinces. The provinces covering areas separated by land were further divided artificially. For example, the province covering the north subtropical Pacific and the province covering the north subtropical Atlantic ~~were was~~ set as one province in the original output of SOM, but ~~it was~~ ere mainly separated by ~~The the~~ North American continent. So, we divided the province into two new provinces. The final version includes ~~total~~ 11 biogeochemical provinces. In this study, the coastal area was not involved, and the boundary was defined as 200 m depth. In addition, the $p\text{CO}_2$ mapping based on SOM-defined provinces tends to be less smooth near the border of different biogeochemical provinces, with an obvious border-line appearing. However, applying ~~of~~ different predictors may make this problem worse. To obtain a smoother distribution, we defined ~~that~~ the area within 5-five 1x1 grids of province boundaries as a “boundary area”. Samples in the boundary area will be used as training samples in all adjacent provinces (Fig. S1). But this definition does not change the actual spatial coverage of each province, only bringings more training samples near the province boundary.

2.3 Stepwise FFNN algorithm

For finding a better combination of $p\text{CO}_2$ predictors, a stepwise Feed-forward neural networks (FFNN) algorithm was constructed. The FFNN ~~is composed of~~ comprises four ~~main~~ parts, ~~which are namely input:~~ input, hidden, summation, and output layer (Fig. 1). The input layer is designed to pass the inputs to the hidden layer, and the number of neurons is equal to the dimensions of the input matrix p . The hidden layer includes 25 neurons in the FFNN model, with ~~the a~~ tan-sigmoid function as the transfer function. The input p is multiplied by a matrix of weights (w_1 in Fig. 1), and the inner product between the result and a bias matrix (b_1 in Fig. 1) is calculated as the input of the transfer function in the first hidden layer. In the summation layer, the transfer function f_2 is ~~a pure~~ linear function. The output of the hidden layer is multiplied by another matrix of weights and summed. All bias and weights matrixes were randomly assigned ~~in at~~ the beginning of FFNN training. The randomly assigned bias

and weights matrixes, the number of training samples, and the sort order of training samples in the input matrix p define where the FFNN starts training in errors space. The practice of FFNN changes when these conditions change. Here we fixed the training samples and set one constant random number stream in the-MATLAB to ensure that the difference between the MAE based on different predictors entirely stems from the predictor differences. The random number was randomly chosen. When using different random number streams, several predictors at the end of the output list of the stepwise FFNN algorithm differed. However, the leading predictors were consistent, and the different predictors were also related. The fixed random number makes all networks using different predictors start training from the same point at the error space when comparing the performance of each predictor, thus the way that the bias and weights matrixes randomly assigned were steady, avoiding the appearance of inconsistent results when the algorithm repeats. The random number was chosen randomly.

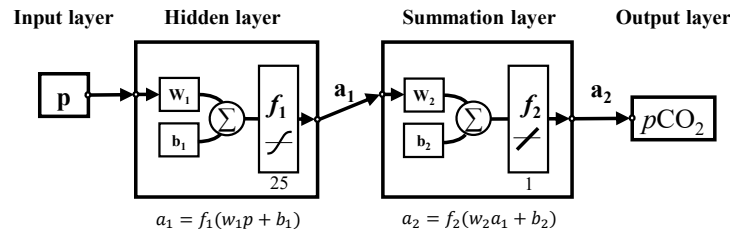


Figure 1. The structure of feed-forward neural network. p : input matrix; w : weighted matrix; b : bias matrix; Σ : sum; f_1 : tan-sigmoid transfer function; f_2 : pure-linear function; a : output matrix.

In the stepwise part, predictors of $p\text{CO}_2$ are going to be added and removed one by one, and which predictors will be finally used in the $p\text{CO}_2$ predicting is determined according to the real-time change of predicting error. The mean absolute error (MAE) difference that before and after adding or removing one indicator in the input of FFNN, calculated using a K-fold cross validation method, was used to estimate the performance of each indicator-predictor in the FFNN predicting. Although the root Root-Mmean-Squared eError (RMSE) was widely used for the validation of machine learning methods, Compared-compared to the MAE, the RMSE was more sensitive to a few extreme samples, which were generally deviated far from the FFNN predicting values, resulting in a considerable huge-discrepancy between the FFNN outputs and $p\text{CO}_2$ observations sometimes up to hundreds of μatm . A higher weight may-might be put on these few extreme samples than other samples in the predictor selection if the performance of each indicator-predictor was estimated by RMSE in the stepwise FFNN algorithm. To avoid the higher weight on these few extreme samples, the MAE was used instead for the internal performance loss function in the stepwise FFNN algorithm.

The basic principle of the stepwise FFNN algorithm was adding each indicator predictor from a set of indicator predictors into the inputs of FFNN and removing each redundant predictor indicator from the inputs successively to reduce the MAE between the FFNN outputs and SOCAT $p\text{CO}_2$ values in the fastest way, until no decrease in the MAE appearing appeared (Fig. 2), where the predictor indicator having no contribution to the reducing of the prediction error was considered as redundant.

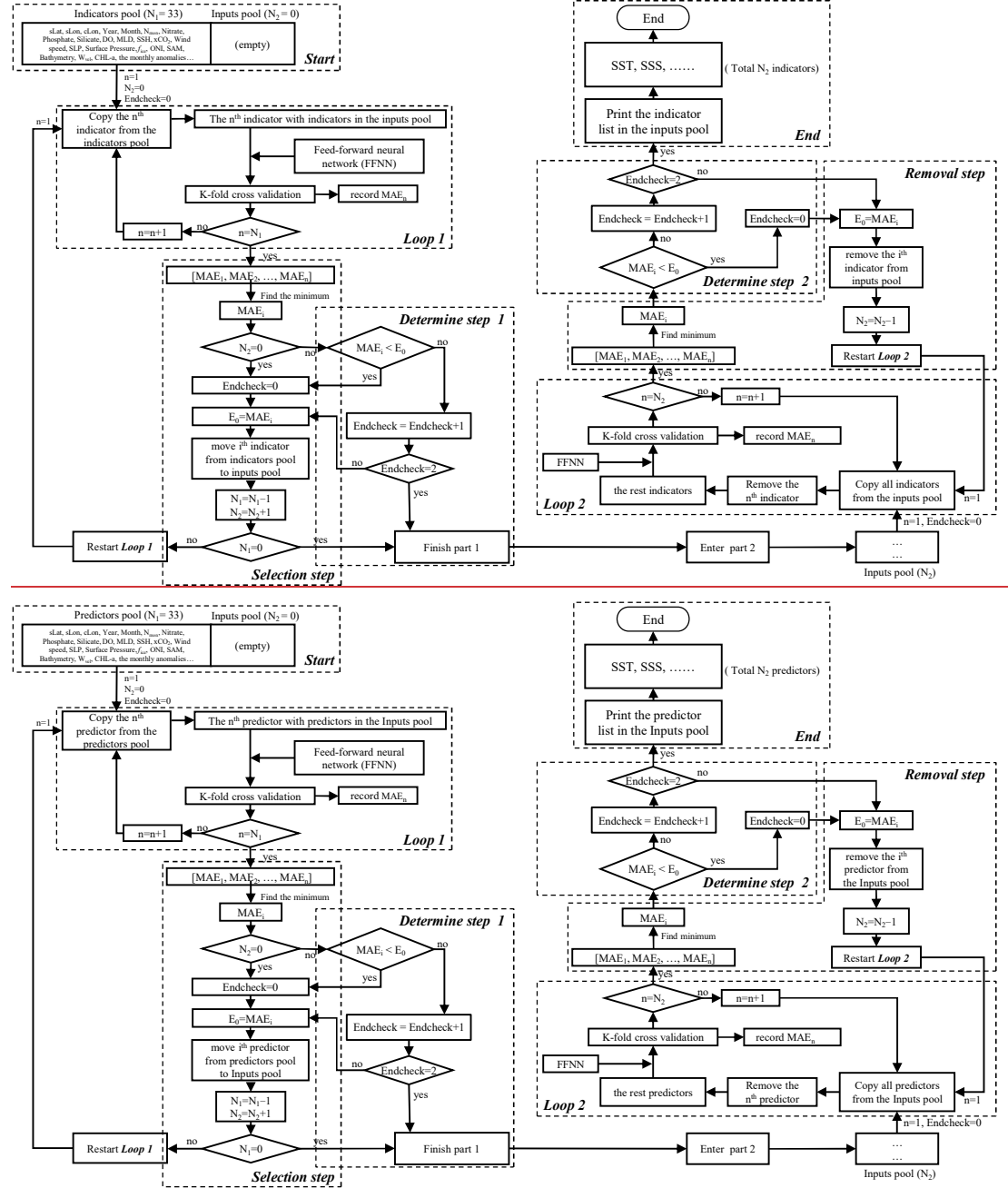


Figure 2. The procedure of the stepwise FFNN algorithm. The flow-chart is following follows an order of “left top – left bottom – right bottom – right top”. The meaning of Indicator Predictors pool: store all indicator predictors waiting to be tested; Inputs pool: store indicator predictors that was were temporally considered as good predictors; Loop 1 and Loop 2: calculate the MAE when each

~~indicatorpredictor~~ was added ~~as predictors~~ or removed; *Selection step*: add good predictors to the *Inputs pool*; *Removal step*: remove predictors from the *Inputs pool* if removing lead to MAE decrease; *Determine step*: check if the process reach end condition. N_1 and N_2 : number of ~~indicatorpredictors~~ in the *IndicatorPredictors pool* and *Inputs pool*, respectively; E_0 : lowest MAE in the last iteration of *Loop 1* or *Loop 2*; *Endcheck*: the number of iterations that E_0 continuously increased.

~~In—At~~ the beginning of the stepwise FFNN algorithm, all available ~~indicatorpredictors~~ were put into a matrix, referred to as ~~indicators~~ *IndicatorPredictors pool* (Start in Fig. 2), ~~where each of the rows. Each row~~ represents one ~~indicatorpredictor~~, and each ~~of the~~ columns represents one SOCAT sample. In this work, we collected 33 ~~indicatorpredictorsparameters~~ for the test, that is, the ~~indicators~~ *IndicatorPredictors pool* matrix has 33 rows. Meanwhile, a matrix, referred to as ~~inputs~~ *Inputs pool* (Start in Fig. 2), was set up to store ~~indicatorpredictors~~ with good performance, where good performance means that adding these ~~indicatorpredictors-as predictors~~ can significantly decrease the MAE between SOCAT pCO_2 measurements and FFNN pCO_2 predictions. Then a loop of K-fold validation test ~~run-ran~~ out to calculate the MAE ~~that-when~~ predicting pCO_2 by each ~~one-indicatorpredictor~~ in the ~~indicators~~ *IndicatorPredictors pool* in the first step (*Loop 1* in the Fig. 2). Thus ~~total~~ 33 MAE values were obtained ~~totally~~, and the minimum was recorded as E_0 . The ~~indicatorpredictor that-corresponding corresponds~~ to the minimum ~~of all~~ MAE values was moved from the ~~indicators~~ *IndicatorPredictors pool* to the ~~inputs-Inputs pool~~ (*Selection step* in the Fig. 2). After that, the ~~loop-Loop 1~~ restarted, i.e., the second step started with one ~~indicatorpredictor~~ removed to the inputs pool and the rest 32 ~~indicatorpredictors~~ waiting to be tested. Then, ~~32 MAE values of predicting the~~ pCO_2 ~~was predicted usingby~~ each ~~one—~~ of the rest ~~32 indicatorpredictors~~ in the ~~indicatorpredictors~~ pool with the addition of all ~~indicatorpredictors~~ in the inputs pool, ~~and 32 MAE values~~ were calculated out. If the MAE in the lowest situation, represented by the MAE_i , decreased compared to the E_0 , the i^{th} ~~indicatorpredictor~~ was considered ~~as-a good indicator-predictor~~ and ~~was~~ moved from the ~~indicatorpredictors~~ pool to the inputs pool ~~as-well~~. Then the value of E_0 was replaced by the MAE_i (*Selection step* in the Fig. 2). The part 1, including ~~loop-Loop 1~~, *Selection step*, and *Determine step 1* in the Fig. 2, was repeated ~~until no predictor was left in the IndicatorPredictors pool or no decrease of E_0 can be found no matter which two indicatorpredictors were added in the next two steps. that-the good indicators were selected out in one-by-one step and moved to the inputs pool in the way that the E_0 decreases in the fastest way, until no~~

indicator was left in the indicators pool or no decrease can be found no matter which indicator was added in the next two steps (*Determine step 1* in the Fig. 2). At this time, the part 1 of the stepwise FFNN algorithm finished, and all indicatorpredictors left in the *indicators-IndicatorPredictors* pool were considered redundant. The loop K-fold validation in the second part ran out in a the opposite way that the MAE was calculated with the indicatorpredictors were removed from the inputs-Inputs pool one by one to decrease E_0 in the way that the E_0 decreases the fastest (*Loop 2* in Fig. 2). The second part was aimed to remove the indicatorpredictor that can be represented by other indicatorpredictors in the inputs pool (*Removal step* in the Fig. 2), and finished in the similar condition that no significant decrease can be found no matter which indicatorpredictor was removed in the next two steps (*Determine step 2* in the Fig. 2).

2.4 $p\text{CO}_2$ product

Dataset of predictorsparameters except for Chl-a start since 1992 or earlier, while Chl-a data ranges from August 2002 to the present. In each one of the provinces, the stepwise FFNN algorithm was run out once first based on all samples covered by Chl-a data; then the algorithm was run out secondly based on samples and all predictorsindicators except Chl-a and $\text{Chl-a}_{\text{anom}}$ in the year that Chl-a gridded data was not available. The $p\text{CO}_2$ mapping in the year that Chl-a gridded data was not available was carried out based on the predictors selected in the second run. Then the final product was built based on two FFNNs, one trained for the period from August 2002 to August 2019 using one predictor set including Chl-a or $\text{Chl-a}_{\text{anom}}$, and the second one for the period from January 1992 to July 2002 using the second predictor set without Chl-a and $\text{Chl-a}_{\text{anom}}$. Although the performance may improve with the number of neurons increasing, the influence of the number of neurons on the performance of FFNN $p\text{CO}_2$ prediction remains unclear. To further decrease the predicating error between FFNN outputs and SOCAT measurements, the number of neurons was improved by an error test in each province. The number of neurons increased from 5 to 300 (the increment was five during 5-50 and ten during 50-100 and fifty during 100-300). and Then the corresponding MAE values of each size were recorded, and then the number of neurons with the lowest MAE was applied. This test avoided the appearance of insufficient learning capacity for complex nonlinear relationships due to too few neurons and the overfitting problem due to too many neurons. Finally, based on the predictorsindicators selected by the stepwise FFNN algorithm and improved FFNN size, a monthly global $1^\circ \times 1^\circ$ surface ocean $p\text{CO}_2$ product from January 1992 to August 2019 was constructed.

2.5 Validation

To better estimate the predicting error of FFNN, the MAE and ~~additionally~~ the RMSE, which ~~was~~ ~~were~~ widely used in previous researches, were calculated using a K-fold cross validation method. To avoid overfitting caused by a lack of independence between the training ~~samples~~ and testing samples, ~~we put~~ the SOCAT samples ~~were put~~ in chronological order and then divided ~~them~~ into ~~the~~ group of years (~~Table-Fig. 1~~) (Gregor et al., 2019). In this paper, the value of K was set as 4. Thus, among every 4 ~~four~~ neighboring years, three group samples were used ~~for to~~ training ~~the~~ FFNN model, and the rest ~~one of group~~ was used for testing. Total 4 iterations were carried out, where testing year changed in each iteration. After 4 iterations finished, all samples ~~have been~~ ~~were~~ used for testing only once, and the MAE and RMSE between FFNN output and the testing samples ~~was~~ ~~were~~ calculated. The performance of the predictor selection algorithm was estimated by comparing the MAE and RMSE results of the FFNN based on ~~predictors selected by the~~ stepwise ~~FFNN algorithm~~ ~~selected indicators~~ with the result based on ~~predictors indicators~~—used in previous researches in each biogeochemical province (Table 2). All validation groups were applied with ~~the~~ same FFNN and same samples from SOCAT, with the only differences in predictors. ~~The~~ ~~s~~ Same K-fold validation procedure was applied for three validation groups based on different $p\text{CO}_2$ predictors. Thus, three results were generated to estimate whether the stepwise FFNN algorithm can effectively find ~~a~~ better combination of $p\text{CO}_2$ predictors. Finally, the $p\text{CO}_2$ data generated in all validation groups were further compared with the completely independent observations from the Hawaii Ocean Time-series (HOT, 22° 45'N, 158° 00'W, since October 1988) (Dore et al., 2009), Bermuda Atlantic Time-series Study (BATS, 31°50'N, 64°10'W, since October 1988) (Bates, 2007) and The European Station for Time Series in the Ocean Canary Islands (ESTOC, 29°10'N, 15°30'W, from 1995 to 2009) (González-Dávila and Santana-Casiano, 2009) time-series station. ~~The $p\text{CO}_2$ at HOT and BAT were estimated from TA and DIC, and $p\text{CO}_2$ at ESTOC were directly measured.~~ These observations were not included in the SOCAT dataset.

~~Table 1. The procedure of K-fold validation.~~

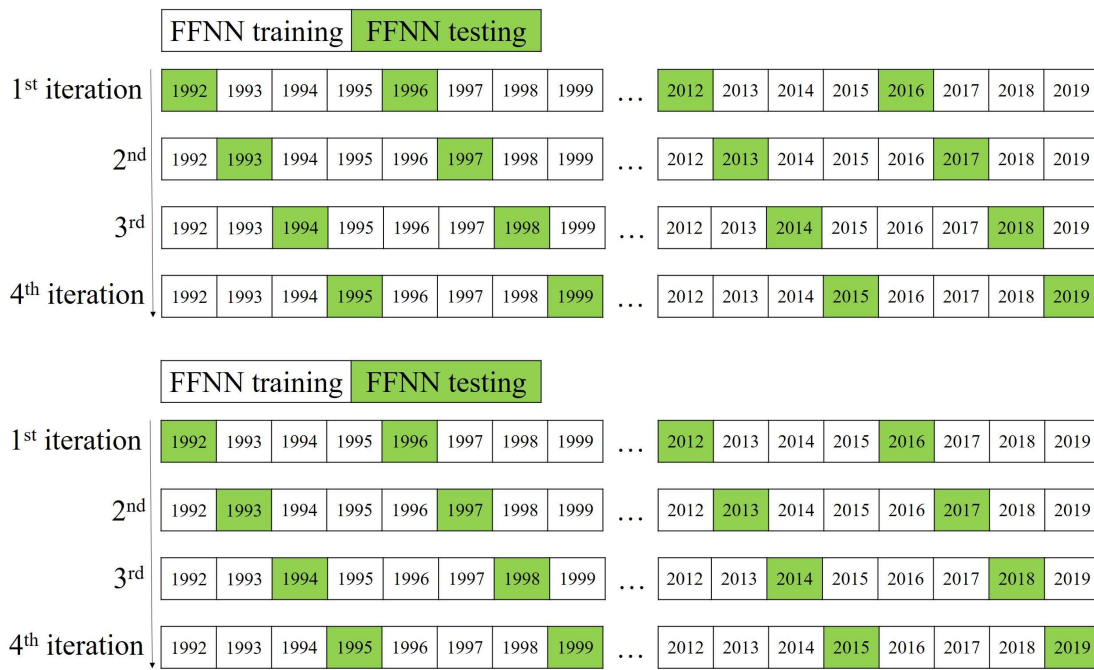


Table 3. The procedure of K-fold validation.

(The K value was set as 4, so iterations repeated four times until all samples ~~have been~~ set as testing samples once. In each iteration, samples in 7 years were set as testing samples (green cells) and in the rest 21 years as training samples (white cells) to increase the ~~independence~~independency.)

Table 2. Validation group using different predictors

Validation group	Predictor
FFNN1	Predictors Indicators selected by stepwise FFNN algorithm
FFNN2	SST, SSS, log ₁₀ (MLD), Chl-a Chl-a , xCO ₂ , SST _{anom} , SSS _{anom} , xCO ₂ _{anom} , Chl-a Chl-a _{anom} , log ₁₀ (MLD) _{anom} (Landschützer et al., 2014)
FFNN3	SST, SSS, SSH, MLD, xCO ₂ , Chl-a Chl-a , SSS _{anom} , SST _{anom} , SSH _{anom} , Chl-a Chl-a _{anom} , MLD _{anom} , xCO ₂ _{anom} , sLat, sLon, cLon (Denvil-Sommer et al., 2019)

(The FFNN performance of three groups with different predictors of $p\text{CO}_2$ were compared; to test the result of stepwise FFNN algorithm. Predictors in the group FFNN1 were selected using stepwise FFNN algorithm, and predictors in the group FFNN2 were selected from Landschützer et al. (2014), and in the group FFNN3 from Denvil-Sommer et al. (2019).)

3 Results and discussion

3.1 Biogeochemical provinces and corresponding predictors of $p\text{CO}_2$

11 biogeochemical provinces generated from the SOM method after the separated

small 'island' was removed and the province separated by lands was divided manually (Fig. 34). The results of the stepwise FFNN algorithm in each province ~~were~~ are shown in ~~the~~ Table 3. The ~~predictors~~ indicators were listed in the order that the stepwise FFNN algorithm printed recommended predictors out. The ~~predictor~~ indicator printed earlier was relatively more recommended and played an important role in predicting the prediction of $p\text{CO}_2$ based on FFNN. Applying ~~of these indicators as the~~ predictors of ~~surface ocean $p\text{CO}_2$~~ effectively decreased the predicting error between the FFNN outputs and $p\text{CO}_2$ values from validation samples, ~~t~~. Thus it is reasonable to consider that these ~~predictors~~ indicators were highly related to the drivers of $p\text{CO}_2$ and its variability. Predictors Indicators representing sampling positions were also listed as recommended predictors in some provinces, including latitude, longitude, and sampling time, suggesting that relatively steady spatial or temporal variability patterns of surface ocean $p\text{CO}_2$ existed in these biogeochemical provinces. For example, the predictor month was considered recommended in most provinces, especially P4 subpolar Atlantic and P5 north subtropical Atlantic. ~~For example, month was considered as a recommended predictor in most provinces. Especially in the province P4 subpolar Atlantic and P5 north subtropical Atlantic, the parameter month was relatively more recommended.~~ While $p\text{CO}_2$ in these areas regularly peaked and bottomed out in summer and winter (Takahashi et al., 2009; Landschützer et al., 2016; Landschützer et al., 2020). Similarly, the sine of latitude and the sine and cosine of longitude were listed as recommended predictors of $p\text{CO}_2$ in most provinces, suggesting ~~an~~ meridional or zonal uniformly varying obvious spatial distribution pattern of $p\text{CO}_2$, which was not learned sufficiently by the FFNN model from existing ~~indicators-measured predictors~~ and the ~~predictors indicators~~ related to the spatial position were applied as supplementary.

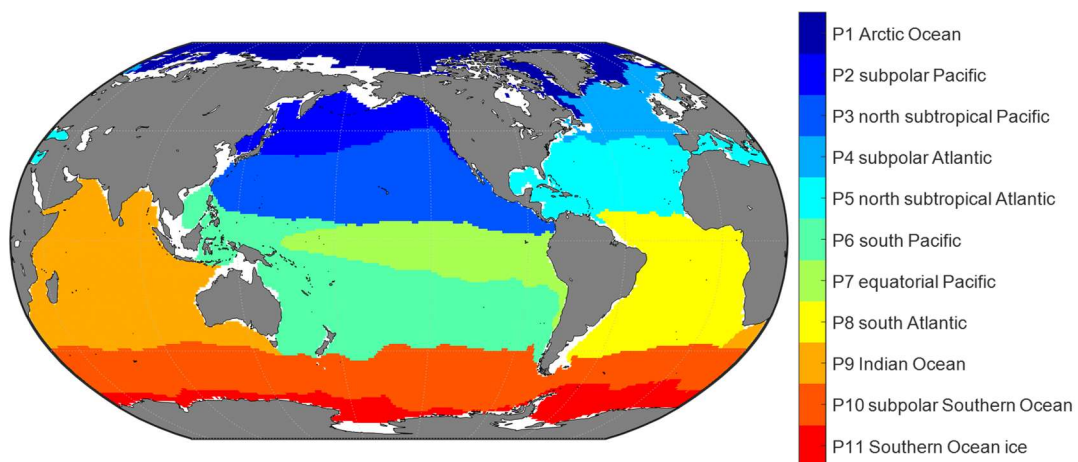


Figure 34. The map of biogeochemical provinces based on SOM.

As basic ~~predictorsparameters~~ highly related to the ocean environment, the temperature and salinity was considered as parts of the most important predictors of surface ocean $p\text{CO}_2$, and was applied in the $p\text{CO}_2$ prediction in almost all previous relating researches based on various method (Jo et al., 2012; Signorini et al., 2013; Landschützer et al., 2014; Marrec et al., 2015; Chen et al., 2016; Moussa et al., 2016; Chen et al., 2017; Laruelle et al., 2017; Zeng et al., 2017; Chen et al., 2019; Denvil-Sommer et al., 2019). The results of the stepwise FFNN algorithm also supported this. The temperature was listed as a recommended predictor in all biogeochemical provinces, suggesting that temperature was ~~the~~ one of the most critical important drivers of $p\text{CO}_2$ and its variability in these provinces. Similarly, ~~the results of from the~~ stepwise FFNN algorithm provides evidence for the importance of salinity in ~~the predication of predicting~~ $p\text{CO}_2$, which was also listed as a predictor in most provinces. The dry air mixing ratio of atmospheric CO_2 ($x\text{CO}_2$) and the monthly anomaly of $x\text{CO}_2$ were also recommended predictors in most ~~of the~~ biogeochemical provinces, suggesting that the exchange of CO_2 across the sea-air interface was also an important driver of surface ocean $p\text{CO}_2$. As a widely used predictor in the $p\text{CO}_2$ prediction, the chlorophyll-a concentration (~~Chl-a~~CHL-a) played an essential important role in fitting the influence of biological activities on $p\text{CO}_2$ in previous researches (Landschützer et al., 2014; Zeng et al., 2017; Laruelle et al., 2017; Denvil-Sommer et al., 2019). Especially in the province P10 subpolar Southern Ocean and P11 Southern Ocean ice, the ~~Chl-a~~CHL-a was listed as the most recommended predictor in the result of the stepwise FFNN algorithm. While in some other provinces (P1 Arctic Ocean and P5 north subtropical Atlantic), the ~~Chl-a~~CHL-a ~~were was~~ considered redundant that no effective decrease of MAE between FFNN outputs and $p\text{CO}_2$ measurements appeared when ~~Chl-a~~CHL-a data was used. Similar ~~with to~~ the period that ~~Chl-a~~CHL-a was not available (represented by the subscript 'b'), the phosphate, nitrate, silicate, or dissolved oxygen were recommended instead. In the province P1 Arctic Ocean, the silicate concentration and temperature were considered ~~as~~ the most crucial predictor of $p\text{CO}_2$.

Table 3. Predictors in each biogeochemical province

Province	Predictors ion the order selected by of the stepwise FFNN algorithm <u>output</u>
P1 Arctic Ocean	Silicate, SST, Wind speed, SSS, $\log_{10}(\text{MLD})$, SSS_{anom} , sLat, month, $\text{W}_{\text{vel}}(65\text{m})$, $\log_{10}(\text{MLD})_{\text{anom}}$, $x\text{CO}_2$, cLon, Bathymetry, SSH
P2 subpolar Pacific ^a	Nitrate, Chl-a <u>CHL-a</u> , SSS, $x\text{CO}_2$, cLon, SST, $\log_{10}(\text{MLD})$, sLon, sLat, month
P2 subpolar Pacific ^b	Nitrate, $x\text{CO}_{2\text{anom}}$, sLon, SST, sLat, $\log_{10}(\text{MLD})$, cLon, SSS, SSH_{anom} , DO, $\text{W}_{\text{vel}}(195\text{m})$, Bathymetry, Silicate

P3 north subtropical Pacific _a	log ₁₀ (MLD), N _{mon} , SSH, SST, sLon, sLat, SSS, Bathymetry, month, log ₁₀ (MLD) _{anom} , cLon, Surface pressure, W _{vel} (105m), Chl-a CHL-a, DO, SSH _{anom} , xCO ₂ _{anom}
P3 north subtropical Pacific _b	log ₁₀ (MLD), xCO ₂ , sLat, sLon, SST, Surface pressure, cLon, SSS, W _{vel} (5m), N _{mon} , log ₁₀ (MLD) _{anom} , month, Phosphate, xCO ₂ _{anom} , W _{vel} (105m)
P4 subpolar Atlantic _a	month, sLat, cLon, SST, Year, Chl-a CHL-a, DO, SSS _{anom} , W _{vel} (195m), SSH, log ₁₀ (MLD), Bathymetry, SSS
P4 subpolar Atlantic _b	month, xCO ₂ , DO, Wind speed, log ₁₀ (MLD), W _{vel} (195m), sLon, Bathymetry, W _{vel} (5m), SST, Phosphate, Year, N _{mon}
P5 north subtropical Atlantic	month, Year, SST, sLon, sLat, SSS, SST _{anom} , SSH, Bathymetry, W _{vel} (5m), cLon, W _{vel} (65m), log ₁₀ (MLD) _{anom}
P6 south Pacific _a	SST, sLon, xCO ₂ _{anom} , sLat, SSS, month, Phosphate, Chl-a CHL-a, Chl-a CHL-a _{anom} , W _{vel} (65m), log ₁₀ (MLD), log ₁₀ (MLD) _{anom} , Nitrate, Bathymetry
P6 south Pacific _b	xCO ₂ , sLat, SSS, SST, Phosphate, SLP, xCO ₂ _{anom} , sLon, cLon, W _{vel} (105m), W _{vel} (65m), DO, Bathymetry, SSH, SAM
P7 _a equatorial Pacific	Nitrate, xCO ₂ , sLat, SSS, SST, cLon, xCO ₂ _{anom} , log ₁₀ (MLD), sLon, Chl-a CHL-a, Phosphate, W _{vel} (5m), W _{vel} (105m), W _{vel} (195m)
P7 _b equatorial Pacific	SST, SSS, Year, sLat, month, cLon, SSH, Bathymetry, W _{vel} (65m), xCO ₂
P8 south Atlantic _a	sLat, xCO ₂ _{anom} , SSS, log ₁₀ (MLD), Chl-a CHL-a, SSH _{anom} , W _{vel} (195m), cLon, SST, W _{vel} (65m), Bathymetry, Nitrate
P8 south Atlantic _b	SST, xCO ₂ , cLon, sLat, SSS, Silicate, SSH, log ₁₀ (MLD), sLon
P9 Indian Ocean _a	SST, cLon, sLat, Nitrate, W _{vel} (65m), log ₁₀ (MLD), SLP, Chl-a CHL-a, Year, log ₁₀ (MLD) _{anom} , SSH _{anom}
P9 Indian Ocean _b	SLP, month, sLon, xCO ₂ _{anom} , SST, Silicate, W _{vel} (65m)
P10 subpolar Southern Ocean _a	Chl-a CHL-a, log ₁₀ (MLD), N _{mon} , SSS, SST, Bathymetry, SSH _{anom} , W _{vel} (5m), Chl-a CHL-a _{anom} , xCO ₂
P10 subpolar Southern Ocean _b	Wind speed, xCO ₂ _{anom} , SSS, Phosphate, log ₁₀ (MLD), W _{vel} (65m), Bathymetry, SST, month
P11 Southern Ocean ice _a	Chl-a CHL-a, sLon, Bathymetry, SSS, SSH, SST, Nitrate, cLon, sLat
P11 Southern Ocean ice _b	month, DO, SST, SSH, sLat, Nitrate, sLon, SSS, W _{vel} (195m), Silicate, SSH _{anom}

*: Due to insufficient coverage of ~~Chl-a~~CHL-a data in the polar areas and during the period before 2002, ~~in the provinces that Chl-a~~ ~~CHL-a~~ or ~~Chl-a~~CHL-a_{anom} were selected as predictors, the pCO₂ data was divided into two periods. The period ~~that with Chl-a~~CHL-a data available was represented by the subscript 'a', such as P2_a, including global grids from 2002 to 2019 except polar grids in winter. The period ~~that with Chl-a~~CHL-a data ~~not un~~available was represented by the subscript 'b', such as P2_b, including global grids from 1992

to 2001 and additionally some polar grids in winter from 1992 to 2019.

3.2 $p\text{CO}_2$ product

Based on the predictors given by the stepwise FFNN algorithm in each biogeochemical province, a FFNN size (representing the number of neurons in the hidden layer) improving validation was applied to further decrease the predication error further. The MAE values based on the same samples and FFNN model with a different number of neurons were calculated, then the number of neurons corresponding to the lowest MAE were applied (Fig. 4a5a). The MAE in most provinces tends to decrease first and then increase when the number of neurons in the hidden layer of the FFNN model increased from 5 to 300. Based on the variation of MAE with the number of neurons in the FFNN hidden layer, the optimal FFNN size in each province was considered as the number of neurons when the MAE was lowest. The result and corresponding MAE were are shown in Fig. 4b5b. After applying optimal FFNN size in each province, The the MAE and RMSE of global estimates between predicted $p\text{CO}_2$ and measurements from SOCAT v2020 further decreased to 11.32 and 17.99 μatm_2 respectively after applying optimal FFNN size in each province.

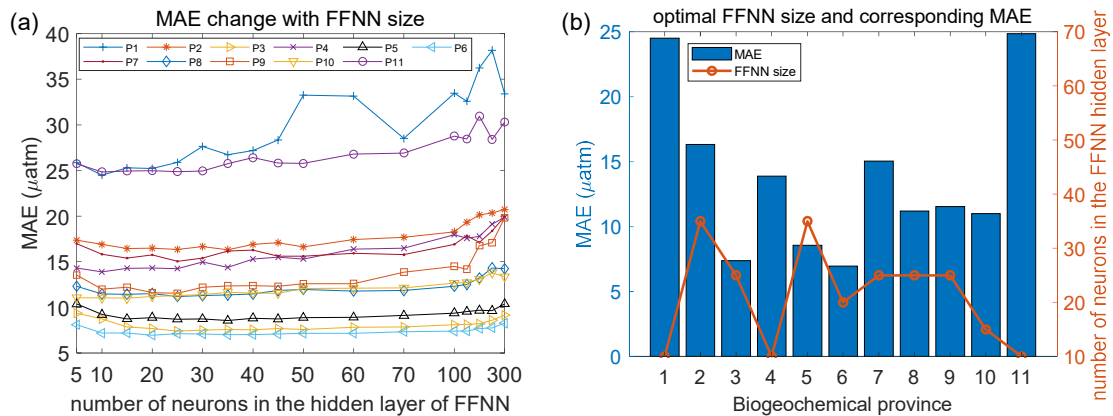


Figure 45. MAE of different FFNN size in each biogeochemical province. a): MAE between predicted $p\text{CO}_2$ and SOCAT observations were was calculated using the same samples and FFNN with a different number of neurons. b): the optimal FFNN size was referring refers to the number of neurons when MAE is lowest.

Then the RMSE and mean residuals in each grid were calculated based on the K-fold cross validation method. In most grids, the RMSE was lower than 10 μatm_2 and the mean residuals was close to zero (Fig. 56). However, the prediction error in the north subpolar Pacific, the eastern equatorial Pacific, and the Southern Ocean near the Antarctic continent was obviously significantly higher than in other areas. Also, the distribution of mean residuals suggested that surface ocean $p\text{CO}_2$ in the Indian Ocean

tends to be overestimated by the FFNN models. While in other regions the distribution of mean residuals was more discrete, and no obvious pattern was found.

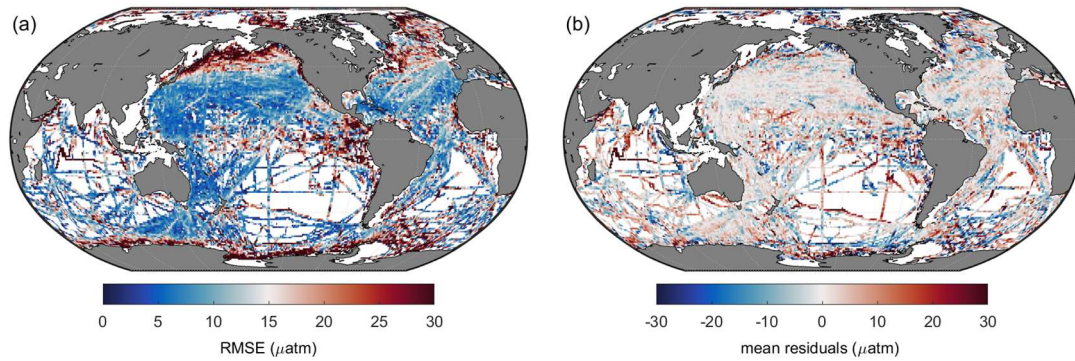


Figure 56. Global maps of (a) RMSE and (b) mean residuals between predicted $p\text{CO}_2$ and SOCAT observations

3.3 Validation of the stepwise FFNN algorithm based on SOCAT samples

Validation based on the K-fold cross validation method suggested that most FFNN outputs were quite close to the $p\text{CO}_2$ values from SOCAT v2020 samples (Fig. 67). Comparing the results based on a different combination of predictors, the results of FFNN1 (based on stepwise FFNN algorithm, this paper) and FFNN3 (based on 15 predictors from Denvil-Sommer et al. 2019) were more precise than that of FFNN2 (based on 10 predictors from Landschützer et al. 2014). The plots in the result of FFNN1 were most concentrated along the $y=x$ line, suggesting extremely close FFNN outputs with the measured $p\text{CO}_2$ values from SOCAT, with the RMSE of 17.99 μatm in the global open oceans. The RMSE of FFNN1 was lower than that of FFNN2 (22.95 μatm) and FFNN3 (19.17 μatm).

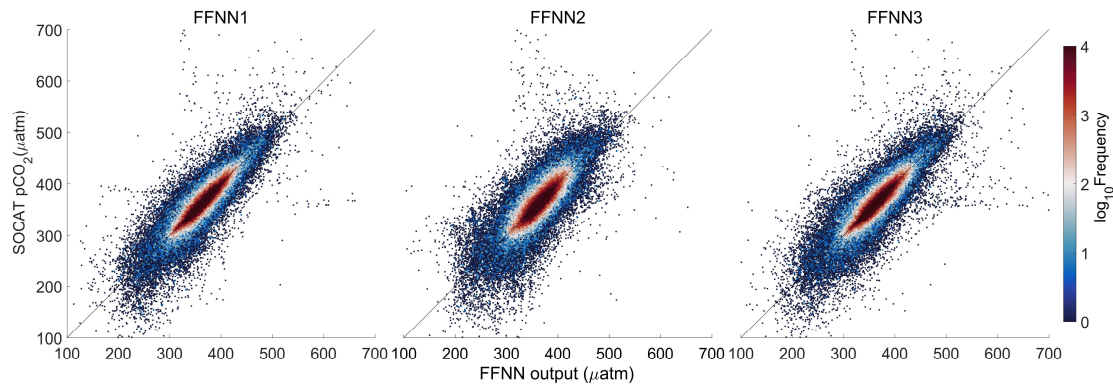


Figure 67. Comparison of FFNN predicted $p\text{CO}_2$ with SOCAT $p\text{CO}_2$. FFNN1 was based on predictors selected by the stepwise-FFNN algorithm. FFNN2 and FFNN3 were based on predictors from Landschützer et al., 2014 and Denvil-Sommer et al., 2019, respectively.

For specific comparison of accuracy in each province, the MAE of FFNN1 was

lower in most provinces (Table 4), except for the relatively close results between the FFNN1 and FFNN3 in parts of provinces. The MAE of FFNN1 in the province P9 Indian Ocean was significantly lower than that of the other validation groups, suggesting a better combination of predictors highly related to the drivers of surface ocean $p\text{CO}_2$ and its variability in the Indian Ocean. Compared with FFNN2 and FFNN3, the predictors of FFNN1 added surface pressure and W velocity of ocean currents, and abandoned the monthly anomalies of other predictors/indicators in the province P9 Indian Ocean. The low relevance between $p\text{CO}_2$ and part of the monthly anomalies, such as SSS_{anom} and SST_{anom} , may be responsible for significantly lower MAE of FFNN1. Adding redundant predictors/indicators may cause misleading in the learning of the FFNN model on the contrary. The MAE and RMSE differences between FFNN1 and FFNN3 in some provinces were relatively small. The reason for higher MAE and RMSE showed by the FFNN2 may be the application of latitudes and longitudes as predictors in both the FFNN1 and FFNN3 but not in the FFNN2. In the province P10 subpolar Southern Ocean, latitudes and longitudes were considered not good predictors by the stepwise FFNN algorithm, and the results of three validation groups were extremely close.

Table 4. Performance of the $p\text{CO}_2$ prediction based on different predictors

Province	FFNN size	MAE (μatm)			RMSE (μatm)		
		FFNN1	FFNN2	FFNN3	FFNN1	FFNN2	FFNN3
P1 Arctic Ocean (9856)	10	24.50	32.32	26.87	32.27	43.68	35.08
P2 subpolar Pacific (30516)	35	16.32	20.63	16.67	24.32	29.87	25.03
P3 north subtropical Pacific (56367)	25	7.39	12.16	7.95	11.33	17.75	11.88
P4 subpolar Atlantic (29595)	10	13.89	16.91	14.73	21.06	24.29	22.27
P5 north subtropical Atlantic (45358)	35	8.55	12.28	9.00	12.80	17.86	13.72
P6 south Pacific (31803)	20	6.96	9.94	7.24	9.86	14.64	11.00
P7 equatorial Pacific (11233)	25	15.05	19.55	15.49	20.98	27.61	21.10
P8 south Pacific (10259)	25	11.19	15.07	12.43	17.10	20.87	17.66
P9 Indian Ocean (7440)	25	11.54	13.78	15.49	17.15	22.89	28.29
P10 subpolar Southern Ocean (21206)	15	11.00	11.76	12.14	16.61	17.22	17.66
P11 Southern Ocean ice (10683)	10	24.84	29.26	25.74	34.73	40.42	35.22
Global (264316)		11.32	15.08	12.06	17.99	22.95	19.17

(FFNN1 was based on predictors selected by the stepwise-FFNN algorithm. FFNN2 and FFNN3

were based on predictors from Landschützer et al., 2014 and Denvil-Sommer et al., 2019, respectively. The lowest MAE and RMSE between different validation groups was shown in bold.

3.4 Validation based on independent observations

The FFNN outputs based on a different combination of predictors were compared with independent observations from the Ocean Time-series (HOT) (Dore et al., 2009), Bermuda Atlantic Time-series Study (BATS) (Bates, 2007), and The European Station for Time Series in the Ocean Canary Islands (ESTOC) (González-Dávila and Santana-Casiano, 2009) (Fig. 78). Compared with the independent observations from the HOT station, the three validation groups both show close results, which were also similar ~~with each other~~ in the seasonal and interannual variability of $p\text{CO}_2$. From 1992 to 2019, the RMSE between FFNN1 outputs and HOT observations was only 9.29 μatm , lower than the 10.85 μatm of FFNN2 and the 10.70 μatm of FFNN3. The monthly mean $p\text{CO}_2$ of FFNN2 during winter was lower than the HOT observations and $p\text{CO}_2$ values of other validation groups, while the FFNN1 and FFNN3 outputs were closer to the HOT observations. MAE between predicted $p\text{CO}_2$ and HOT observations ~~were~~ was also lower in the validation group FFNN1, which was only 7.17 μatm , compared to the 8.61 μatm of FFNN2 and the 8.44 μatm of FFNN3. Higher bias generated in the winter bottom and summer peak, ~~which was showed~~ shown more obviously in the monthly average of $p\text{CO}_2$ (Fig. 78b). Compared with other validation groups, the result of FFNN1 was closer to the monthly average values of the HOT observations. ~~The s~~ Same conclusion can be obtained in the ESTOC and BATS station located in the province P5 north subtropical Atlantic. The RMSE between FFNN1 outputs and independent observations ~~were~~ was 13.03 μatm in the BATS station and 11.35 μatm in the ESTOC station, lower than ~~that of~~ other validation groups. The RMSE between FFNN2 outputs and independent observations was 16.15 μatm in the BATS station and 14.51 μatm in the ESTOC station. For the group FFNN3, the RMSE was 13.09 μatm in the BATS station and 13.01 μatm in the ESTOC station. All results were extremely close to the independent observations, but the RMSE and MAE of FFNN1 were lower. Similar ~~with~~ to the situation in the HOT station, the FFNN1 was most close and the FFNN3 second. Based on the better performance of FFNN1, in which the predictors selected by stepwise FFNN algorithm were used, we may conclude that the stepwise FFNN algorithm can effectively find a better combination of predictors to fit the diver of surface ocean $p\text{CO}_2$ and obtained a lower error.

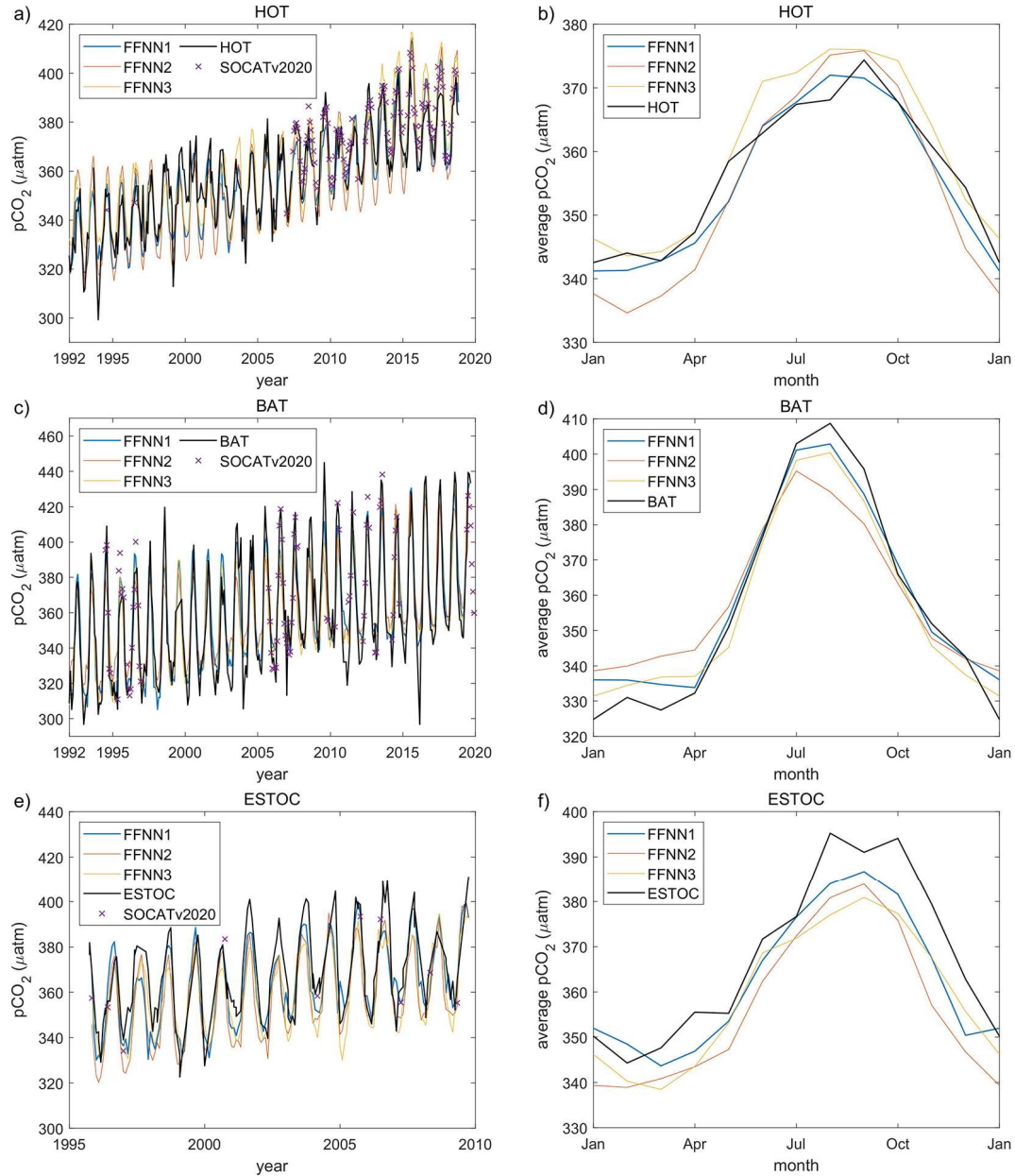


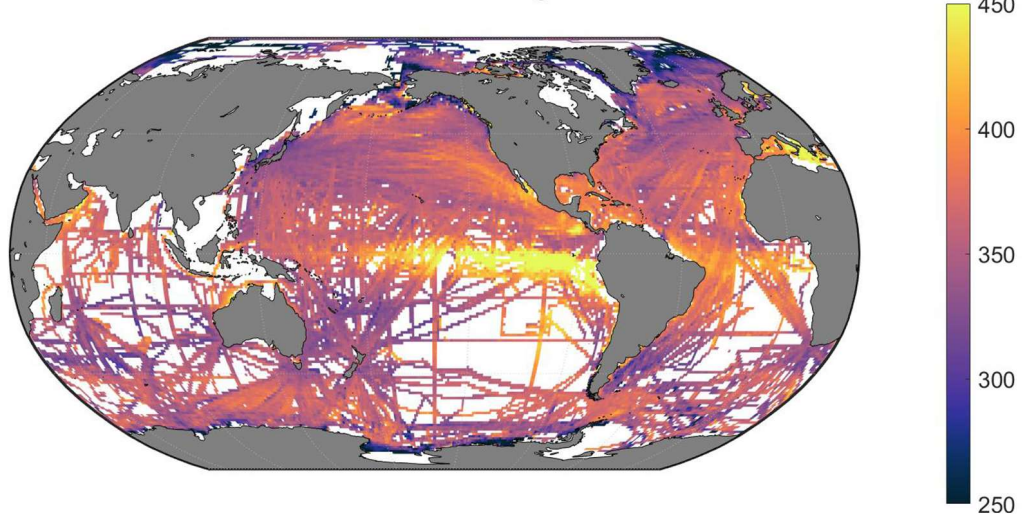
Figure 78. Validation based on independent observation from time series stations. a) and b): the Hawaii Ocean Time-series (HOT) (Dore et al., 2009); c) and d): the Bermuda Atlantic Time-series Study (BATS) (Bates, 2007); e) and f): the European Station for Time Series in the Ocean Canary Islands (ESTOC) (González-Dávila and Santana-Casiano, 2009) time-time-series station. FFNN1 was based on predictors selected by the stepwise-FFNN algorithm. FFNN2 and FFNN3 were based on predictors from Landschützer et al., 2014 and Denvil-Sommer et al., 2019, respectively. SOCATv2020 represents the monthly mean $p\text{CO}_2$ of SOCAT observations in the corresponding grids of each time series station.

3.5 Climatological spatial distribution

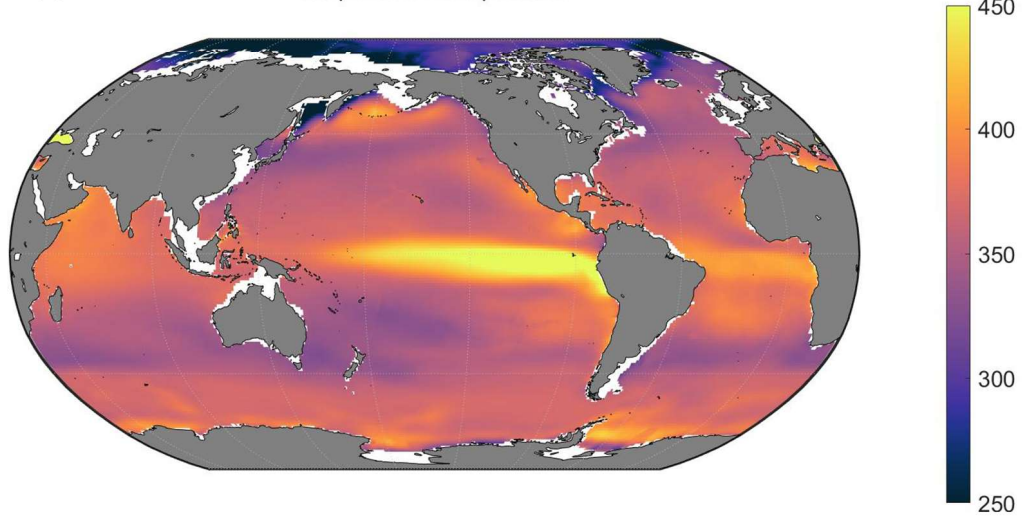
The climatological average distribution of $p\text{CO}_2$ suggested a significant spatial

variability (Fig. 89), ~~which is~~ consistent with the average distribution of SOCAT observations. In the Pacific Ocean, the high $p\text{CO}_2$ areas showed by the stepwise-FFNN product (Fig. 8b9b), including the equatorial areas, east temperate areas, and north subpolar areas, were highly consistent with the SOCAT datasets (Fig. 8a9a). Similarly, the distribution of $p\text{CO}_2$ in the Atlantic Ocean was also close. However, the stepwise-FFNN product suggested lower $p\text{CO}_2$ average values in the Arctic and higher values in the Southern Ocean near the Antarctic continent. Compared with the previous climatology product (Landschützer et al., 2020), the stepwise FFNN product ~~have has~~ similar spatial patterns with high $p\text{CO}_2$ in the eastern equatorial Pacific and equatorial Atlantic: inconsistent spatial distribution also existed in the Arctic and parts of the Southern Ocean near the Antarctic continent. The differences between the stepwise-FFNN product and the previous climatology product may be caused by differences in methods or SOCAT dataset versions used. In comparison, ~~While~~ lower average values of the SOCAT dataset in the Southern Ocean may be caused by the undersampling in winter. The global spatial distribution pattern of the stepwise FFNN $p\text{CO}_2$ product was basically well consistent with previous climatology product and SOCAT dataset, suggesting that $p\text{CO}_2$ predicting based on regional ~~different-specific~~ predictors selected by the stepwise FFNN algorithm was better than that based on the globally same predictors.

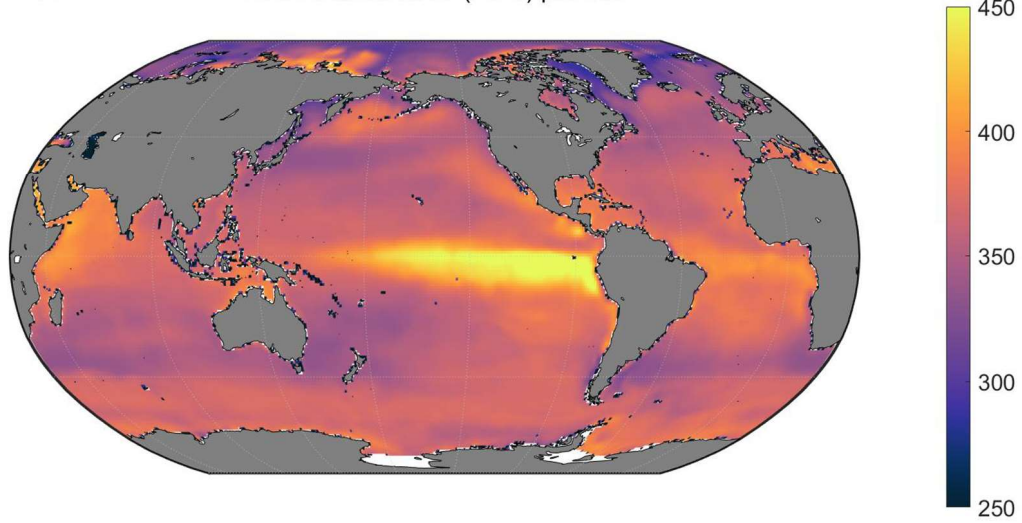
(a) SOCAT v2020 average



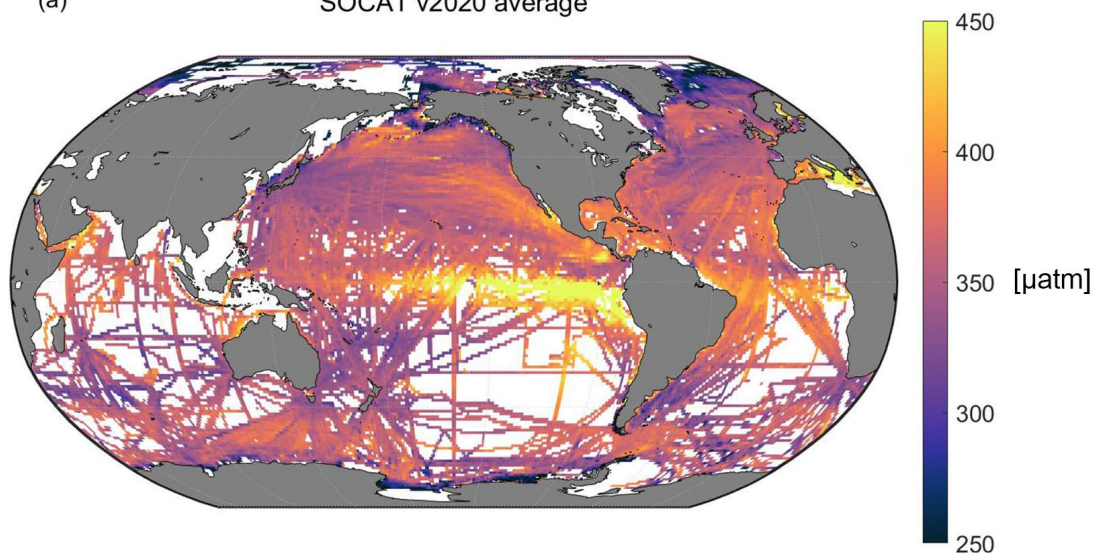
(b) stepwise FFNN product



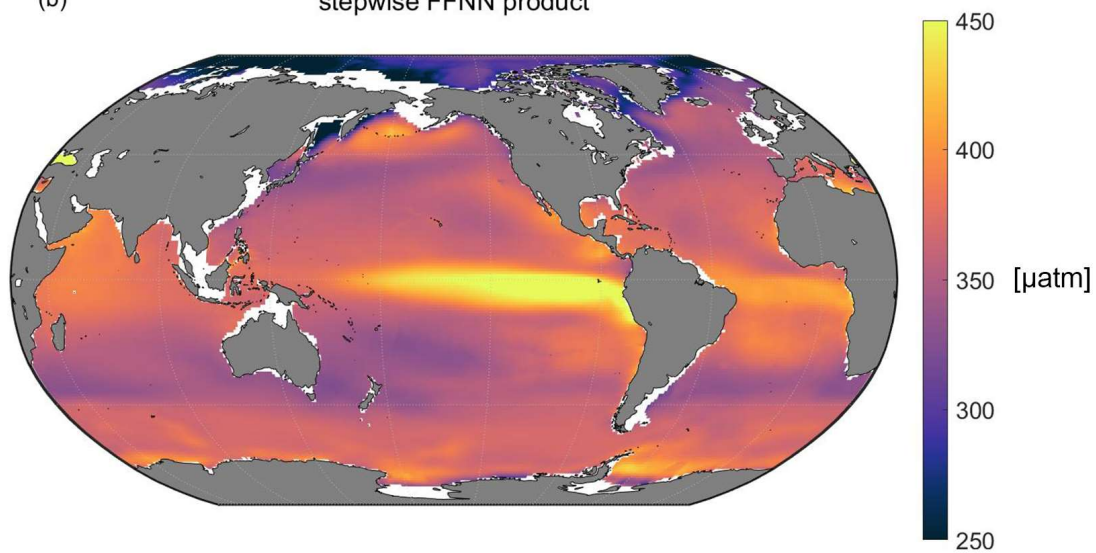
(c) Landschutzer et al. (2020) product



(a) SOCAT v2020 average



(b) stepwise FFNN product



(c) Landschutzer et al. (2020) product

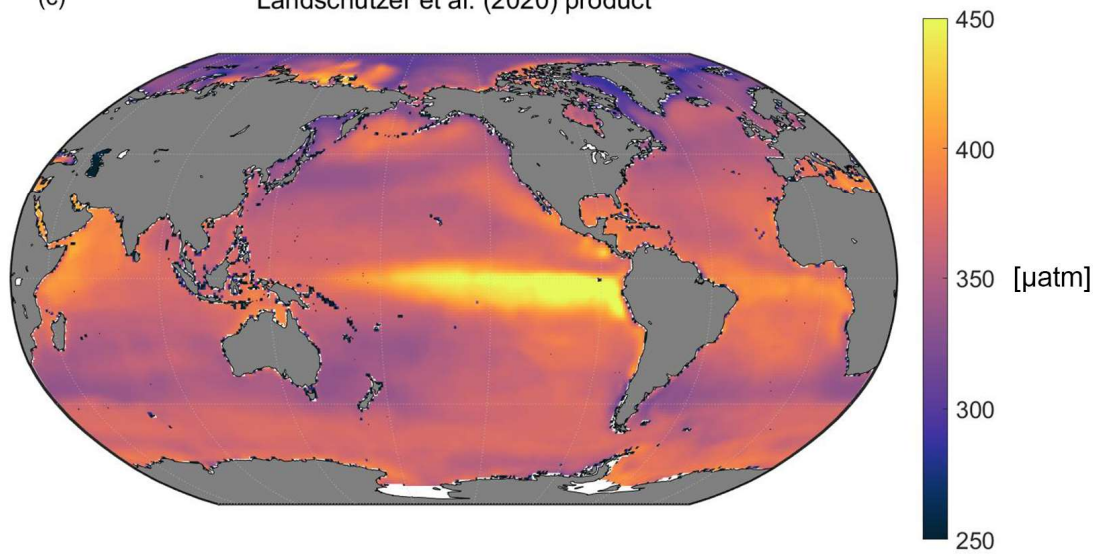


Figure 89. Comparison between long term average of a): SOCAT v2020 dataset, b): the stepwise FFNN $p\text{CO}_2$ product, and c): previous climatology product adapted from Landschützer et al., 2020.

4. Conclusions

A stepwise FFNN algorithm was constructed to ~~decreasing-decrease~~ the predicting error in the surface ocean $p\text{CO}_2$ mapping by finding better combinations of $p\text{CO}_2$ predictors in each biogeochemical province defined by SOM method, based on which a monthly $1^\circ \times 1^\circ$ gridded global open-oceanic surface ocean $p\text{CO}_2$ product from January 1992 to August 2019 was constructed. Our work provided a statistical way of predictor selection for all researches based on relationship fitting by machine learning methods. The validation based on the SOCAT dataset and independent observations ~~and~~ shows that using regional-specific predictors selected by the stepwise FFNN algorithm retrieved lower predicting error than ~~using~~ globally same predictors. This stepwise FFNN algorithm can ~~be also~~ be used in $p\text{CO}_2$ mapping researches for higher resolution and coastal regions, and ~~also in~~ other data mapping researches using SOM or other region dividing methods. The preparation ~~prepare~~ work was only collecting as many ~~predictors~~ parameters, which are possibly related to the target data and need to be sufficiently available in time and space. However, high predicting error in particular ~~special~~ regions ~~still~~ remains to be improved, such as polar regions and equatorial Pacific. Since ~~the result of~~ the stepwise FFNN algorithm's result largely depends on the way how biogeochemical provinces are divided, improving ~~of the~~ SOM step is still necessary. Besides, the FFNN can be replaced by any suitable type of neural networks. A possible way to improve the performance of the stepwise FFNN algorithm is to modify the structure of FFNN or to use ~~better~~ networks with more sophisticated architecture and to use different learning algorithms. In the future work, the stepwise FFNN algorithm with possible improvement will be attempted in the mapping of other ~~parameters~~ products, such as total alkalinity and pH, to provide ~~more~~ sufficient data support for studies on ocean acidification and carbon cycling.

Code and data availability

The stepwise FFNN algorithm (as a .m file for MATLAB) and the global $1^\circ \times 1^\circ$ gridded surface ocean $p\text{CO}_2$ product since from January 1992 to August 2019 (as a NetCDF file) generated during this study is available from the Institute of Oceanology of the Chinese Academy of Sciences Marine Science Data Center at <http://dx.doi.org/10.12157/iocas.2021.0022> or directly at <http://english.casodc.com/data/metadata-special-detail?id=1418424272359075841>.

Author contribution

Ma Jun, Yuan Huamao and Duan Liqin collected the dataset of $p\text{CO}_2$ predictors, and Qu baoxiao and Wang Yanjun was contributed in the synthesis of datasets. Zhong Guorong, Li Xuegang and Song Jinming designed the predictor selection algorithm and performed the reconstruction of $p\text{CO}_2$ product. Wang Fan, Zhang Bin, Sun Xiaoxia, Zhang Wuchang, and Wang Zhenyan were contributed in the further improving. Zhong Guorong prepared the manuscript with contributions from all co-authors.

Competing interests

The authors declare that they have no conflict of interest.

Acknowledgement

This work was supported by The National Key Research and Development Program of China (No. 2017YFA0603204), the Strategic Priority Research Program of the Chinese Academy of Sciences (No. XDA19060401), National Natural Science Foundation of China (No. 91958103 and No. 42176200), and Natural Science Foundation of Shandong Province (ZR2020YQ28). We thank SOCAT for sharing the $f\text{CO}_2$ observation data. The Surface Ocean CO_2 Atlas (SOCAT) is an international effort, endorsed by the International Ocean Carbon Coordination Project (IOCCP), the Surface Ocean Lower Atmosphere Study (SOLAS) and the Integrated Marine Biosphere Research (IMBeR) program, to deliver a uniformly quality-controlled surface ocean CO_2 database. The many researchers and funding agencies responsible for the collection of data and quality control are thanked for their contributions to SOCAT. We thank NASA Goddard Space Flight Center, Ocean Ecology Laboratory, Ocean Biology Processing Group for sharing the Chlorophyll concentration data.

References

Bakker, D. C. E., Pfeil, B., Landa, C. S., Metzl, N., O'Brien, K. M., Olsen, A., Smith, K., Cosca, C., Harasawa, S., Jones, S. D., Nakaoka, S.-i., Nojiri, Y., Schuster, U., Steinhoff, T., Sweeney, C., Takahashi, T., Tilbrook, B., Wada, C., Wanninkhof, R., Alin, S. R., Balestrini, C. F., Barbero, L., Bates, N. R., Bianchi, A. A., Bonou, F., Boutin, J., Bozec, Y., Burger, E. F., Cai, W.-J., Castle, R. D., Chen, L., Chierici, M., Currie, K., Evans, W., Featherstone, C., Feely, R. A., Fransson, A., Goyet, C., Greenwood, N., Gregor, L., Hankin, S., Hardman-Mountford, N. J., Harlay, J., Hauck, J., Hoppema, M., Humphreys, M. P., Hunt, C., Huss, B., Ibanez, J. S. P., Johannessen, T., Keeling, R., Kitidis, V., Koertzinger, A., Kozyr, A., Krasakopoulou, E., Kuwata, A., Landschützer, P., Lauvset, S. K., Lefevre, N., Lo Monaco, C., Manke, A., Mathis, J. T., Merlivat, L., Millero, F. J., Monteiro, P. M. S., Munro, D. R., Murata, A., Newberger, T., Omar, A. M., Ono, T., Paterson, K., Pearce, D., Pierrot, D., Robbins, L. L., Saito, S., Salisbury, J., Schlitzer, R., Schneider, B., Schweitzer, R., Sieger, R., Skjelvan, I., Sullivan, K. F., Sutherland, S. C., Sutton, A. J., Tadokoro, K., Telszewski, M., Tuma, M., van Heuven, S. M. A. C., Vandemark, D., Ward, B., Watson, A. J., and Xu, S.: A multi-decade record of high-quality $f\text{CO}_2$ data in version

616 3 of the Surface Ocean CO₂ Atlas (SOCAT), *Earth System Science Data*, 8, 383–413,
 617 10.5194/essd-8-383-2016, 2016.

618 Bates, N. R.: Interannual variability of the oceanic CO₂ sink in the subtropical gyre of
 619 the North Atlantic Ocean over the last 2 decades, *Journal of Geophysical Research:*
 620 *Oceans*, 112, 2007.

621 Broullón, D., Pérez, F. F., Velo, A., Hoppema, M., Olsen, A., Takahashi, T., Key, R. M.,
 622 Tanhua, T., González-Dávila, M., Jeansson, E., Kozyr, A., and van Heuven, S. M. A.
 623 C.: A global monthly climatology of total alkalinity: a neural network approach,
 624 *Earth System Science Data*, 11, 1109–1127, 10.5194/essd-11-1109-2019, 2019.

625 Broullon, D., Perez, F. F., Velo, A., Hoppema, M., Olsen, A., Takahashi, T., Key, R. M.,
 626 Tanhua, T., Magdalena Santana-Casiano, J., and Kozyr, A.: A global monthly
 627 climatology of oceanic total dissolved inorganic carbon: a neural network approach,
 628 *Earth System Science Data*, 12, 1725–1743, 10.5194/essd-12-1725-2020, 2020.

629 Chen, L. Q., Xu, S. Q., Gao, Z. Y., Chen, H. Y., Zhang, Y. H., Zhan, J. Q., and Li, W.:
 630 Estimation of monthly air-sea CO₂ flux in the southern Atlantic and Indian Ocean
 631 using in-situ and remotely sensed data, *Remote Sensing of Environment*, 115, 1935–
 632 1941, 10.1016/j.rse.2011.03.016, 2011.

633 Cheng L. and J. Zhu: Benefits of CMIP5 multimodel ensemble in reconstructing
 634 historical ocean subsurface temperature variation, *Journal of Climate*, 29(15), 5393–
 635 5416, 10.1175/JCLI-D-15-0730.1, 2016.

636 Cheng L., K. Trenberth, J. Fasullo, T. Boyer, J. Abraham, J. Zhu: Improved estimates
 637 of ocean heat content from 1960 to 2015, *Science Advances*, 3, e1601545, 2017.

638 Cheng L., K. E. Trenberth, N. Gruber, J. P. Abraham, J. Fasullo, G. Li, M. E. Mann, X.
 639 Zhao, Jiang Zhu: Improved estimates of changes in upper ocean salinity and the
 640 hydrological cycle. *Journal of Climate*, 33, 10357–10381, 10.1175/JCLI-D-20-
 641 0366.1, 2020.

642 Chen, S., Hu, C., Barnes, B. B., Wanninkhof, R., Cai, W.-J., Barbero, L., and Pierrot,
 643 D.: A machine learning approach to estimate surface ocean *p*CO₂ from satellite
 644 measurements, *Remote Sensing of Environment*, 228, 203–226,
 645 10.1016/j.rse.2019.04.019, 2019.

646 Chen, S. L., Hu, C. M., Byrne, R. H., Robbins, L. L., and Yang, B.: Remote estimation
 647 of surface *p*CO₂ on the West Florida Shelf, *Continental Shelf Research*, 128, 10–25,
 648 10.1016/j.csr.2016.09.004, 2016.

649 Chen, S. L., Hu, C. M., Cai, W. J., and Yang, B.: Estimating surface *p*CO₂ in the northern
 650 Gulf of Mexico: Which remote sensing model to use?, *Continental Shelf Research*,
 651 151, 94–110, 10.1016/j.csr.2017.10.013, 2017.

652 Commerce, U. D. o., Administration, N. O. a. A., and Center, N. G. D.: 2-minute
 653 Gridded Global Relief Data (ETOPO2v2).
 654 <http://www.ngdc.noaa.gov/mgg/fliers/06mgg01.html>, 2006.

655 Dee, D. P., Uppala, S. M., Simmons, A. J., Berrisford, P., Poli, P., Kobayashi, S., Andrae,
 656 U., Balmaseda, M. A., Balsamo, G., Bauer, P., Bechtold, P., Beljaars, A. C. M., van
 657 de Berg, L., Bidlot, J., Bormann, N., Delsol, C., Dragani, R., Fuentes, M., Geer, A.
 658 J., Haimberger, L., Healy, S. B., Hersbach, H., Holm, E. V., Isaksen, L., Kallberg, P.,
 659 Kohler, M., Matricardi, M., McNally, A. P., Monge-Sanz, B. M., Morcrette, J. J., Park,

B. K., Peubey, C., de Rosnay, P., Tavorato, C., Thepaut, J. N., and Vitart, F.: The ERA-Interim reanalysis: configuration and performance of the data assimilation system, *Q J Roy Meteor Soc*, 137, 553-597, 10.1002/qj.828, 2011.

Denvil-Sommer, A., Gehlen, M., Vrac, M., and Mejia, C.: LSCE-FFNN-v1: a two-step neural network model for the reconstruction of surface ocean $p\text{CO}_2$ over the global ocean, *Geoscientific Model Development*, 12, 2091-2105, 10.5194/gmd-12-2091-2019, 2019.

Dore, J. E., Lukas, R., Sadler, D. W., Church, M. J., and Karl, D. M.: Physical and biogeochemical modulation of ocean acidification in the central North Pacific, *Proceedings of the National Academy of Sciences*, 106, 12235-12240, 2009.

Friedlingstein, P., Jones, M. W., O'Sullivan, M., Andrew, R. M., Hauck, J., Peters, G. P., Peters, W., Pongratz, J., Sitch, S., Le Quere, C., Bakker, D. C. E., Canadell, J. G., Ciais, P., Jackson, R. B., Anthoni, P., Barbero, L., Bastos, A., Bastrikov, V., Becker, M., Bopp, L., Buitenhuis, E., Chandra, N., Chevallier, F., Chini, L. P., Currie, K. I., Feely, R. A., Gehlen, M., Gilfillan, D., Gkritzalis, T., Goll, D. S., Gruber, N., Gutekunst, S., Harris, I., Haverd, V., Houghton, R. A., Hurtt, G., Ilyina, T., Jain, A. K., Joetzjer, E., Kaplan, J. O., Kato, E., Goldewijk, K. K., Korsbakken, J. I., Landschützer, P., Lauvset, S. K., Lefevre, N., Lenton, A., Lienert, S., Lombardozzi, D., Marland, G., McGuire, P. C., Melton, J. R., Metzl, N., Munro, D. R., Nabel, J. E. M. S., Nakaoka, S.-I., Neill, C., Omar, A. M., Ono, T., Peregon, A., Pierrot, D., Poulter, B., Rehder, G., Resplandy, L., Robertson, E., Rodenbeck, C., Seferian, R., Schwinger, J., Smith, N., Tans, P. P., Tian, H., Tilbrook, B., Tubiello, F. N., van der Werf, G. R., Wiltshire, A. J., and Zaehle, S.: Global Carbon Budget 2019, *Earth System Science Data*, 11, 1783-1838, 10.5194/essd-11-1783-2019, 2019.

Friedrich, T., and Oschlies, A.: Neural network-based estimates of North Atlantic surface $p\text{CO}_2$ from satellite data: A methodological study, *Journal of Geophysical Research-Oceans*, 114, Art. C03020, 10.1029/2007jc004646, 2009.

Garcia, H., Weathers, K., Paver, C., Smolyar, I., Boyer, T., Locarnini, M., Zweng, M., Mishonov, A., Baranova, O., and Seidov, D.: World Ocean Atlas 2018. Vol. 4: Dissolved Inorganic Nutrients (phosphate, nitrate and nitrate+ nitrite, silicate), 2019a.

Garcia, H., Weathers, K., Paver, C., Smolyar, I., Boyer, T., Locarnini, M., Zweng, M., Mishonov, A., Baranova, O., and Seidov, D.: World Ocean Atlas 2018, Volume 3: Dissolved Oxygen, Apparent Oxygen Utilization, and Dissolved Oxygen Saturation, 2019b.

GLOBALVIEW-CO2: Cooperative Atmospheric Data Integration Project - Carbon Dioxide [CD-ROM]. NOAA ESRL, B., Colo. (Ed.), [Available at ftp.cmdl.noaa.gov, path: ccg/co2/GLOBALVIEW, 5th January 2013.], 2011.

González-Dávila, M., and Santana-Casiano, J.: Sea surface and atmospheric $f\text{CO}_2$ data measured during the estoc time series cruises from 1995-2009, CDIAC, Oak Ridge National Laboratory, US Department of Energy, Oak Ridge, Tennessee. doi, 10, 2009.

Gregor, L., Lebehot, A. D., Kok, S., & Scheel Monteiro, P. M. A comparative assessment of the uncertainties of global surface ocean CO_2 estimates using a machine-learning ensemble (CSIR-ML6 version 2019a)–have we hit the wall?. *Geoscientific Model Development*, 12(12), 5113-5136, 2019.

- Hales, B., Strutton, P. G., Saraceno, M., Letelier, R., Takahashi, T., Feely, R., Sabine, C., and Chavez, F.: Satellite-based prediction of $p\text{CO}_2$ in coastal waters of the eastern North Pacific, *Prog Oceanogr*, 103, 1-15, 10.1016/j.pocean.2012.03.001, 2012.
- Huang, B., Thorne, P. W., Banzon, V. F., Boyer, T., Chepurin, G., Lawrimore, J. H., Menne, M. J., Smith, T. M., Vose, R. S., and Zhang, H.-M.: Extended reconstructed sea surface temperature, version 5 (ERSSTv5): upgrades, validations, and intercomparisons, *J Climate*, 30, 8179-8205, 2017.
- Iida, Y., Kojima, A., Takatani, Y., Nakano, T., Midorikawa, T., and Ishii, M.: Trends in $p\text{CO}_2$ and sea-air CO_2 flux over the global open oceans for the last two decades, *J. Oceanogr.*, 71, 637–661, 10.1007/s10872-015-0306-4, 2015.
- Jo, Y. H., Dai, M. H., Zhai, W. D., Yan, X. H., and Shang, S. L.: On the variations of sea surface $p\text{CO}_2$ in the northern South China Sea: A remote sensing based neural network approach, *Journal of Geophysical Research-Oceans*, 117, Artn C08022, 10.1029/2011jc007745, 2012.
- Körtzinger, A.: Determination of carbon dioxide partial pressure ($p\text{CO}_2$), 3rd ed., *Methods of Seawater Analysis*, 3rd edn., 1999.
- Landschützer, P., Gruber, N., Bakker, D. C. E., and Schuster, U.: Recent variability of the global ocean carbon sink, *Glob. Biogeochem. Cycle*, 28, 927-949, 10.1002/2014gb004853, 2014.
- Landschützer, P., Gruber, N., Bakker, D. C. E., Schuster, U., Nakaoka, S., Payne, M. R., Sasse, T. P., and Zeng, J.: A neural network-based estimate of the seasonal to inter-annual variability of the Atlantic Ocean carbon sink, *Biogeosciences*, 10, 7793-7815, 10.5194/bg-10-7793-2013, 2013.
- Landschützer, P., Gruber, N., and Bakker, D. C. E.: Decadal variations and trends of the global ocean carbon sink, *Glob. Biogeochem. Cycle*, 30, 1396-1417, 10.1002/2015gb005359, 2016.
- Landschützer, P., Laruelle, G. G., Roobaert, A., and Regnier, P.: A uniform $p\text{CO}_2$ climatology combining open and coastal oceans, *Earth Syst. Sci. Data Discuss.*, 2020, 1-30, 10.5194/essd-2020-90, 2020.
- Laruelle, G. G., Landschützer, P., Gruber, N., Tison, J. L., Delille, B., and Regnier, P.: Global high-resolution monthly $p\text{CO}_2$ climatology for the coastal ocean derived from neural network interpolation, *Biogeosciences*, 14, 4545-4561, 10.5194/bg-14-4545-2017, 2017.
- Marrec, P., Cariou, T., Mace, E., Morin, P., Salt, L. A., Vernet, M., Taylor, B., Paxman, K., and Bozec, Y.: Dynamics of air-sea CO_2 fluxes in the northwestern European shelf based on voluntary observing ship and satellite observations, *Biogeosciences*, 12, 5371-5391, 10.5194/bg-12-5371-2015, 2015.
- Marshall G J.: Trends in the Southern Annular Mode from observations and reanalyses, *Journal of climate*, 16, 10.1175/1520-0442(2003)016<4134:TITSAM>2.0.CO;2, 4134-4143, 2003.
- Menemenlis, D., Campin, J.-M., Heimbach, P., Hill, C., Lee, T., Nguyen, A., Schodlok, M., and Zhang, H.: ECCO2: High Resolution Global Ocean and Sea Ice Data Synthesis, *Mercator Ocean Quarterly Newsletter*, 2008.

- Moussa, H., Benallal, M. A., Goyet, C., and Lefevre, N.: Satellite-derived CO₂ fugacity in surface seawater of the tropical Atlantic Ocean using a feedforward neural network, *Int J Remote Sens*, 37, 580-598, 10.1080/01431161.2015.1131872, 2016.
- Nakaoka, S., Telszewski, M., Nojiri, Y., Yasunaka, S., Miyazaki, C., Mukai, H., and Usui, N.: Estimating temporal and spatial variation of ocean surface *p*CO₂ in the North Pacific using a self-organizing map neural network technique, *Biogeosciences*, 10, 6093-6106, 10.5194/bg-10-6093-2013, 2013.
- NASA Goddard Space Flight Center, Ocean Ecology Laboratory, Ocean Biology Processing Group. Moderate-resolution Imaging Spectroradiometer (MODIS) Aqua Chlorophyll Data; 2018 Reprocessing. NASA OB.DAAC, Greenbelt, MD, USA. 10.5067/AQUA/MODIS/L3M/CHL/2018, 2018.
- Rödenbeck, C., Bakker, D. C. E., Metzl, N., Olsen, A., Sabine, C., Cassar, N., Reum, F., Keeling, R. F., and Heimann, M.: Interannual sea–air CO₂ flux variability from an observation-driven ocean mixed-layer scheme, *Biogeosciences*, 11, 4599–4613, 10.5194/bg-11-4599-2014, 2014.
- Sabine, C. L., Feely, R. A., Gruber, N., Key, R. M., Lee, K., Bullister, J. L., Wanninkhof, R., Wong, C. S., Wallace, D. W. R., Tilbrook, B., Millero, F. J., Peng, T. H., Kozyr, A., Ono, T., and Rios, A. F.: The oceanic sink for anthropogenic CO₂, *Science*, 305, 367-371, DOI 10.1126/science.1097403, 2004.
- Sarma, V. V. S. S., Saino, T., Sasaoka, K., Nojiri, Y., Ono, T., Ishii, M., Inoue, H. Y., and Matsumoto, K.: Basin-scale *p*CO₂ distribution using satellite sea surface temperature, Chl-a, and climatological salinity in the North Pacific in spring and summer, *Glob. Biogeochem. Cycle*, 20, Artn Gb3005, 10.1029/2005gb002594, 2006.
- Shadwick, E. H., Thomas, H., Comeau, A., Craig, S. E., Hunt, C. W., and Salisbury, J. E.: Air-Sea CO₂ fluxes on the Scotian Shelf: seasonal to multi-annual variability, *Biogeosciences*, 7, 3851-3867, 10.5194/bg-7-3851-2010, 2010.
- Signorini, S. R., Mannino, A., Najjar, R. G., Friedrichs, M. A. M., Cai, W. J., Salisbury, J., Wang, Z. A., Thomas, H., and Shadwick, E.: Surface ocean *p*CO₂ seasonality and sea-air CO₂ flux estimates for the North American east coast, *Journal of Geophysical Research-Oceans*, 118, 5439-5460, 10.1002/jgrc.20369, 2013.
- Takahashi, T., Sutherland, S. C., Feely, R. A., and Wanninkhof, R.: Decadal change of the surface water *p*CO₂ in the North Pacific: A synthesis of 35 years of observations, *Journal of Geophysical Research-Oceans*, 111, Artn C07s05, 10.1029/2005jc003074, 2006.
- Takahashi, T., Sutherland, S. C., Wanninkhof, R., Sweeney, C., Feely, R. A., Chipman, D. W., Hales, B., Friederich, G., Chavez, F., Sabine, C., Watson, A., Bakker, D. C. E., Schuster, U., Metzl, N., Yoshikawa-Inoue, H., Ishii, M., Midorikawa, T., Nojiri, Y., Kortzinger, A., Steinhoff, T., Hoppema, M., Olafsson, J., Arnarson, T. S., Tilbrook, B., Johannessen, T., Olsen, A., Bellerby, R., Wong, C. S., Delille, B., Bates, N. R., and de Baar, H. J. W.: Climatological mean and decadal change in surface ocean *p*CO₂, and net sea-air CO₂ flux over the global oceans, *Deep-Sea Research Part II-Topical Studies in Oceanography*, 56, 554-577, 10.1016/j.dsr2.2008.12.009, 2009.

- Telszewski, M., Chazottes, A., Schuster, U., Watson, A. J., Moulin, C., Bakker, D. C. E., Gonzalez-Davila, M., Johannessen, T., Kortzinger, A., Luger, H., Olsen, A., Omar, A., Padin, X. A., Rios, A. F., Steinhoff, T., Santana-Casiano, M., Wallace, D. W. R., and Wanninkhof, R.: Estimating the monthly $p\text{CO}_2$ distribution in the North Atlantic using a self-organizing neural network, *Biogeosciences*, 6, 1405-1421, DOI 10.5194/bg-6-1405-2009, 2009.
- Wang, Y., Li, X., Song, J., Zhong, G., and Zhang, B.: Carbon Sinks and Variations of $p\text{CO}_2$ in the Southern Ocean from 1998 to 2018 Based on a Deep Learning Approach, *IEEE Journal of Selected Topics in Applied Earth Observations and Remote Sensing*, 2021.
- Watson, A. J., Schuster, U., Shutler, J. D., Holding, T., Ashton, I. G. C., Landschützer, P., Woolf, D. K., and Goddijn-Murphy, L.: Revised estimates of ocean-atmosphere CO_2 flux are consistent with ocean carbon inventory, *Nature Communications*, 11, 10.1038/s41467-020-18203-3, 2020.
- Weiss, R. F.: Carbon dioxide in water and seawater: the solubility of a non-ideal gas, *Marine Chemistry*, 2, 203--215, 1974.
- Zeng, J., Nojiri, Y., Landschützer, P., Telszewski, M., and Nakaoka, S.: A Global Surface Ocean $f\text{CO}_2$ Climatology Based on a Feed-Forward Neural Network, *Journal of Atmospheric and Oceanic Technology*, 31, 1838-1849, 10.1175/jtech-d-13-00137.1, 2014.
- Zeng, J. Y., Nojiri, Y., Nakaoka, S., Nakajima, H., and Shirai, T.: Surface ocean CO_2 in 1990-2011 modelled using a feed-forward neural network, *Geosci Data J*, 2, 47-51, 10.1002/gdj3.26, 2015.
- Zeng, J. Y., Matsunaga, T., Saigusa, N., Shirai, T., Nakaoka, S., and Tan, Z. H.: Technical note: Evaluation of three machine learning models for surface ocean CO_2 mapping, *Ocean Sci*, 13, 303-313, 10.5194/os-13-303-2017, 2017.
- Zhong, G., Li, X., Qu, B., Wang, Y., Yuan, H., and Song, J.: A General Regression Neural Network approach to reconstruct global $1^\circ \times 1^\circ$ resolution sea surface $p\text{CO}_2$, *Acta Oceanol Sin*, 10, 70-79, 10.3969/j.issn.0253-4193.2020.10.007, 2020.